A Comparison of Two Surface Wind Stress Analyses over the Tropical Atlantic during 1980–1987

BOHUA HUANG AND J. SHUKLA

Center for Ocean–Land–Atmosphere Studies (COLA), Institute of Global Environment and Society (IGES), Calverton, Maryland

(Manuscript received 15 October 1993, in final form 10 May 1995)

ABSTRACT

Two sets of monthly sea surface wind stress over the tropical Atlantic Ocean are compared. The datasets are based on the ECMWF analyses during 1980–87 (the E-winds) and the monthly pseudo-wind stress from ship observations for the same period (the S-winds). Our examination shows that both datasets give qualitatively similar mean fields and annual cycles. Quantitatively, the zonal component of the E-winds is larger than that of the S-winds, especially in the winter hemisphere. The strongest southeast trades of the E-winds are also shifted to the east of the strongest southeast trades of the S-winds. In the vicinity of the ITCZ, the E-winds are more zonally oriented so that the convergence zone is not as clearly defined.

Interannually, both datasets show that the northeast trades were gradually strengthening from 1980 to 1986. The southeast trade winds, on the other hand, were anomalously strong during 1981–83, but weak during 1984–86. With the E-winds, the southeast trades decreased gradually during 1981–84, and with the S-winds, the southeast trades are maintained until late 1983, followed by a rapid weakening. In comparison with the E-winds, the S-winds interannual fluctuations over the central and eastern part of the tropical south and equatorial Atlantic are weak.

The sensitivity of an ocean general circulation model to the uncertainty of surface wind forcing as exemplified by these two datasets is examined. It is found that the systematic errors in the mean state and annual cycle of the model simulated sea surface temperature (SST) and upper ocean heat content (HC) are not sensitive to the differences in wind forcings. On the other hand, significantly different fluctuations of both the SSTs and the HCs on interannual timescales are generated by the simulations forced with the two wind data, respectively. A comparison between the observed and simulated SST anomalies shows that both simulations are reasonably close to the observations in the tropical north Atlantic Ocean. In the tropical south Atlantic, the E-winds produce a better simulation of the SST anomalies. Especially, the gradual weakening of the E-winds during 1981–84 produces an SST tendency consistent with observations, which are not shown in the S-winds simulation. However, the E-winds anomalies are poor during 1980–81 as judged by the comparison between the simulated and the observed SST anomalies.

1. Introduction

To understand the ocean circulation and its variability, reliable knowledge of the wind stress at the sea surface is required. However, considerable uncertainties exist in estimating this quantity due to inadequate temporal and spatial sampling of the observations. This causes substantial discrepancies in different wind stress analyses and in ocean model simulations (see, e.g., Harrison et al. 1989).

Traditionally, surface wind stress fields are constructed based on ship wind observations with substantial smoothing and interpolation into data-sparse regions. Using historical ship observations from the past decades, Wyrtki and Meyers (1976), Bunker (1978), Hellerman and Rosenstein (1983), and Harrison (1989) produced climatological monthly mean wind stress fields over the regional and the World Ocean. These climatologies are composites of all available historical observations for each calendar month. However, they still suffer from sampling problems in some regions, such as the Arctic, Antarctic, and Southern Oceans (Hellerman and Rosenstein 1983).

Goldenberg and O'Brien (1981) and Servain et al. (1987) constructed multiyear time series of monthly mean wind stress over the tropical Pacific and Atlantic Oceans. The sampling problem may have a much more serious effect on these monthly fields. Halpern (1988) showed that a monthly mean wind estimate over the tropical ocean with 95% confidence to have accuracy of 1 m s^{-1} needs about nine independent observations. This sampling level is hard to reach in large areas, even in the tropical Atlantic Ocean (Picaut et al. 1985). An error of 1 m s^{-1} in the tropical monthly mean wind corresponds to a wind stress error of 10^{-1} dyn cm^{-2}, without accounting for the effect of aliasing higher fre-

Corresponding author address: Dr. Bohua Huang, Center for Ocean–Land–Atmosphere Studies, Institute of Global Environment and Society, 4041 Powder Mill Road, Suite 302, Calverton, MD 20705-3106.

quency fluctuations. This level of error is not negligible in examining the interannual variability of the tropical surface wind stress.

In the past decade, the technique of data assimilation has been developed in analyzing meteorological observations, in which the inevitable interpolation in data-sparse regions is performed under physical constraints of the numerical weather prediction (NWP) model rather than under single variable statistical analyses. The assimilated analyses produce global coverage with regular 12-h (or shorter) sampling so that the temporal sampling problem in estimating surface wind stress can be reduced. The first description of the climatology of global surface wind stress from assimilated winds near the surface were given by Trenberth et al. (1990) based on the European Centre for Medium-Range Weather Forecasts (ECMWF) twice-daily analyses during 1980–86 and show features different from previous climatologies. Trenberth et al. (1990) claimed that this wind stress climatology is the most reliable climatology over the Southern Ocean.

Few studies have been conducted to investigate interannual fluctuations of the available assimilated surface wind stress data or use them in ocean modeling. One problem of using these data is that the analyzed fields may carry the systematic bias of the NWP models. In particular, the accuracy of present analyses is not high for the Tropics (Trenberth and Olson 1988; Reynolds et al. 1989; Trenberth 1992). Another problem is the spurious temporal fluctuation originated from changes of the assimilation systems and the NWP models (Trenberth and Olson 1988; Trenberth 1992). Bengtsson and Shukla (1988) argued that the reanalyzed datasets with a single analysis–forecast system will produce better datasets to study climate change and interannual variability. A pilot retrospective analysis of 19 months (May 1982–November 1983) of global atmospheric observations has been completed in the Center of Ocean–Land–Atmosphere Studies (Paolino et al. 1995). Recently, long-term reanalysis projects have been announced by some meteorological institutes (e.g., Kalnay and Jenne 1991; Schubert et al. 1993). In this study, we examine how these error sources affect the quality of the analysis from operational assimilation and to what extent operational analyses can be exploited in climate study.

A quantitative comparison is made of two datasets of the sea surface wind stress over the tropical Atlantic Ocean produced from the two analysis approaches described above. One dataset is constructed based on the wind analyses from the ECMWF operational analysis–forecast system, the other is from the Servain et al. (1987) statistical analysis of ship observations. Although both datasets have been examined separately in previous studies (see, e.g., Trenberth et al. 1990; Mestas-Nuñez et al. 1994; Servain et al. 1985; Servain and Legler 1986), there has been no quantitative comparison between them. There has also been no comprehensive assessment of the interannual signals of the wind stress based on the ECMWF analysis in the tropical Atlantic region. In this study, we will emphasize the interannual variability of these two datasets.

Since one of the major usages of the observed surface wind stress is to provide boundary forcings for ocean models in simulating oceanic mean state and variability, it is important to examine how sensitive the model simulations are to the uncertainty of boundary forcing. To address this sensitivity, we force the GFDL ocean general circulation model (Philander and Pacanowski 1986) with these two surface wind stress datasets and examine the difference of the simulated mean upper-ocean thermal structure and its temporal variability. We have also compared the sea surface temperatures (SST) from the two simulations with observations in order to get some insight on the relative accuracy of the two datasets.

The organization of this paper is as follows. A description of the two sea surface wind stress datasets and the ocean model are given in section 2. In section 3, we compare the mean fields and the annual cycles of the two wind stress data and discuss their effect on the OGCM simulations. The interannual variability is discussed in section 4. Section 5 summarizes our main results.

2. Data and model description

a. Surface wind stress

Surface wind stress $\boldsymbol{\tau}$ is obtained from sea surface winds $\mathbf{v}$ based on the bulk aerodynamic formula:

$$\boldsymbol{\tau} = \rho C_D V \mathbf{v}, \tag{1}$$

where V is wind speed, ρ is surface air density, and C_D is drag coefficient. The calculation follows Trenberth et al. (1990) procedure with C_D as a function of the surface wind and a stability factor (for detailed descriptions, see also Large and Pond 1981, 1982). The stability is estimated from COADS (Comprehensive Ocean–Atmosphere Data Set) monthly climatology.

The 1000-mb winds from the ECMWF four-dimensional data assimilation (Hollingsworth et al. 1986) are used to obtain the first stress data (referred to as the E-winds). Global ECMWF analyses are taken from NASA Goddard Flight Center on a twice-daily interval and 2.5° × 2° grid from 0000 UTC 1 January 1980 through 1200 UTC 31 December 1988. The stress fields are calculated over the Atlantic Ocean from 40°S to 60°N. The density (ρ) is derived at each grid point applying the equation of state to the ECMWF data. A monthly mean dataset is constructed by averaging the twice-daily fields within each month. This calculation is the same as Trenberth et al. (1990) except that the version of the ECMWF analyses we used has slightly different resolution and we are interested in interannual variations. We noted that Trenberth et al. (1989b,

1990) evaluated the ECMWF winds over the tropical Pacific and found the divergence field to be poorly reproduced, especially prior to 1983.

The 1000-mb winds (not exactly surface winds) were used for the calculation because the ECMWF data-assimilation system treated ship-observed winds as 1000-mb winds before 9 September 1986, as discussed in detail by Trenberth et al. (1989b). We have chosen to use the ECMWF 1000-mb winds with the same C_D formulation to convert surface wind stress over the ocean after 9 September 1986, although the ECMWF data assimilation that is carried on model σ levels provides both 1000-mb wind and winds at 10-m height above the sea surface. The reason for this choice is to maintain the consistency of the dataset. There is no systematic deviation before and after 1986 within the dataset constructed this way.

According to Trenberth et al. (1990), the ECMWF 1000-mb winds for this period are representative of the surface winds or winds at 10 m about the sea surface, which are usually used to calculate surface wind stress from bulk aerodynamic formula. In fact, a comparative study conducted by Böttger (1982) shows that daily ECMWF 1000-mb wind speeds and those observed at ocean weather ship Lima (57°N, 20°W) are close to each other in both magnitude and variability. There are also additional evidences in support of Trenberth et al. (1990) argument. Janssen et al. (1989) found that accurate wave predictions could be made when the ECMWF 1000-mb winds were treated as 10-m winds in ocean–wave modeling. In fact, surface wind stresses based on 1000-mb winds from the ECMWF and other data analysis systems over the ocean have been widely used in ocean modeling (e.g., Rosati and Miyakoda 1988; Harison et al. 1989; Carton and Huang 1994; Huang et al. 1995). The results seem at least as good as those derived from those using wind stress fields based on ship observed winds only.

On the other hand, there may be shortcomings in constructing surface wind stress this way. Anderson et al. (1991) found that the 1000-mb ECMWF winds correspond to winds at a height of approximately 30 m and thus must be reduced in magnitude to be compared with 10-m measurements. Based on a comparison with wind stress derived from the *Seasat-A* Satellite Scatterometer (SASS) measurements, Mestas-Nuñez et al. (1994) point out that surface wind stress climatology constructed by Trenberth et al. (1990) may overestimate the magnitude of wind stress and should be reduced by 17%. The problem of magnitude, however, seem only significant in the extratropical latitudes. One of the purposes of this comparison is to detect its effect in the Tropics.

The second wind stress dataset is obtained from monthly pseudo-stress ($V\mathbf{v}$) constructed by Servain and collaborators (Servain et al. 1987) from historical ship observations for 1964–87. In their construction, the monthly pseudo-stress was averaged in 5° × 2° boxes from 60°W to the African coast within 20°S–30°N, and objective analysis was done to obtain a gap-free dataset on a 2° × 2° mesh. We calculated the monthly surface wind stress from this dataset by multiplying them with ρ and C_D. Since no suitable observations are available, ρ was fixed as 1.2×10^{-3} g cm^{-3}. Here C_D is derived using monthly COADS climatology and wind speed V from the monthly pseudo wind stress data, assuming fluctuations within a month are small (Trenberth et al. 1989a). We will refer to this stress dataset as the S-winds.

b. *Ocean general circulation model*

The GFDL ocean model used for this study solves the system of primitive equations with the hydrostatic and Bousinesq approximations. Its domain includes the Atlantic Ocean from 30°S to 50°N with zonal resolution of 1° throughout the basin and meridional resolution 1/3° equatorward of 10° and gradually coarser toward higher latitudes. There are 27 levels in the vertical, with a constant interval of 10 m for the upper 100 m. The model basin geometry and topography are realistic, and no-slip condition is prescribed at the coast and artificially at 30°S and 50°N. To minimize the effects of the artificial boundaries, temperature and salinity at higher latitudes is relaxed to monthly climatology. The horizontal mixing and diffusion have constant coefficients (2×10^7 cm^2 s^{-1}), but the coefficients for vertical mixing and diffusion are Richardson number dependent (Pacanowski and Philander 1981). The model is driven by surface wind stress and heat flux.

The wind stress is prescribed forcing at the sea surface. Two experiments were performed with surface forcings from both wind stress data as discussed in last section. For the experiment with the S-wind forcing, the E-winds were placed in model regions beyond where the S-winds are defined. The merging of the two datasets is done after both datasets are linearly interpolated onto appropriate ocean model grids and a smoothing procedure is applied at the boundaries between the two datasets.

The surface heat fluxes include the net solar and longwave radiation, as well as latent and sensible heat fluxes. In the model these are parameterized following Philander and Pacanowski (1986). The net solar radiation is prescribed as a constant of 500 ly day^{-1} within 20°S–20°N, then decreases linearly to 300 ly day^{-1} between 20° and 45° latitudes. The longwave radiation is taken to be constant of 115 ly day^{-1} over the whole basin. The sensible and latent heat fluxes are calculated with the bulk formula from the climatological monthly air temperature, model SST, and surface wind speed. The surface wind speed is determined from the prescribed monthly wind stress forcings with a constant drag coefficient $C_D = 1.4 \times 10^{-3}$. A minimum monthly wind speed of 3.85 m s^{-1} is prescribed to account for the effect of high-frequency wind fluctuations on heat

transfer since both wind speed data are monthly means. In general, the magnitudes of longwave and sensible heat fluxes are smaller than the net solar radiation and latent heat fluxes, and the surface heat balance is mainly between the latter two components. Philander and Pacanowski (1986) and Philander et al. (1987) showed that the upper ocean thermal structure and circulation of the tropical Atlantic and Pacific Ocean can be realistically reproduced using this parameterization.

One should note that not all the processes affecting heat exchange at the sea surface are represented explicitly in this simple heat flux parameterization. For example, the radiative fluxes are zonally uniform without accounting for the contribution of cloudiness distribution. Its effect, however, is not expected to be large because of the way the other components are treated in the parameterization. Specifically, the specified surface air temperature in calculating the latent and sensible heat fluxes plays a much more significant role in controlling the model SST climatology and annual cycle. As pointed out by Seager et al. (1988) and Gent (1991), this specification is similar to including a relaxation to observed SST climatology because in reality surface air temperature closely parallels SST. This restriction should have accomplished most of the effect of a specified climatological cloudiness on heat flux.

The climatological monthly surface air temperature is deliberately used in calculating latent and sensible heat fluxes, although it fluctuates both annually and interannually in reality. The intention is to prevent the specified surface air temperature directly providing the model with information of the observed SST interannual variability since away from the coasts it is the air temperature that adjusts to the SST and not the other way around. Therefore, the only prescribed interannually varying quantity in the heat flux parameterization is the surface wind speed, which modulates the relaxation rate of model SST to the prescribed surface air temperature. In fact, Cayan (1992) showed that wind fluctuations are the major factor driving tropical latent heat anomalies from the annual cycle. The interannual fluctuation of the radiative fluxes is neglected.

Both experiments start from the same initial state, corresponding to an ocean at rest with climatological temperature and salinity in January (Levitus 1982). For both runs, the model is first spun up for six years while forced by corresponding long-term mean monthly wind stress to obtain quasi-equilibrium ocean conditions.

Finally, we point out that the two simulations are designed as identical "twin" experiments in the sense that the only difference between them is in the surface wind–wind stress forcings. To make the study objective, there is no tuning of any parameters in favor of either wind stress forcing. All the model parameters are kept the same as those in Philander and Pacanowski (1986).

3. Mean field and annual cycle

As a background for the interannual fluctuations to be described in next section, we briefly compare the mean states and the annual cycles of the surface wind stress from the two datasets for 1980–87. A monthly climatology of wind stress is constructed by averaging available data for each calendar month. It should be noted that similar climatologies for both datasets have been described before (see, e.g., Trenberth et al. 1990; Servain et al. 1985; Servain and Legler 1986), but here we present a quantitative comparison between the two datasets. We choose to consider the climatology from the entire period of 1980–87 because it seems appropriate to define anomalous fluctuations with respect to the means over the whole period. In the next section we will try to distinguish spurious signals from real interannual variability in the E-winds, including those related to the improvements in analysis.

The E-winds are interpolated to a $2° \times 2°$ longitude–latitude grid and the datasets are compared in their common domain (i.e., 20°S–30°N, 60°W–15°E,) and time interval (1980–87). Mean surface wind stress is characterized in both datasets by the northeast and the southeast trade wind systems located in the Northern and Southern Hemispheres, respectively (Figs. 1a,b). These trade winds converge to the north of the equator, forming the intertropical convergence zone (ITCZ), a "kinematic axis" extending northeastward from the western equatorial Atlantic to the African coast. Apparently, the trade winds are stronger in the E-winds (see the shaded area in Figs. 1a and 1b), which also have an additional maximum at the Senegal coast in comparison with the S-winds. South of the equator, maximum winds are shifted northwestward in the S-winds compared with the E-winds. In the latter, the maximum winds are in the eastern part of the ocean south of 10°S. In the former, on the other hand, the strongest winds are located in the western part of the ocean between the equator and 10°S.

These differences can be more clearly demonstrated in the maps of wind components (Fig. 2). Stronger trades over the open ocean in the E-winds are mostly due to the contribution of its zonal component. The E-winds have larger easterly component over most of the domain, and their differences with the S-winds can be as high as 0.2 dynes cm^{-2} (Figs. 2a,c). The maximum in the E-winds near the African coast is caused by both stronger westward and southward components there (Figs. 2c,d). On the other hand, the S-winds have larger northward component from around the equator to 10°S, as well as stronger easterlies near the Brazilian coast (Figs. 2b,d).

The difference in the meridional components near the equator affects the mean positions of ITCZ in the two datasets. To the west of 25°W, the S-winds converge meridionally to a narrow zone confined to the equator and 5°N, shown as a well-defined ITCZ (Fig.

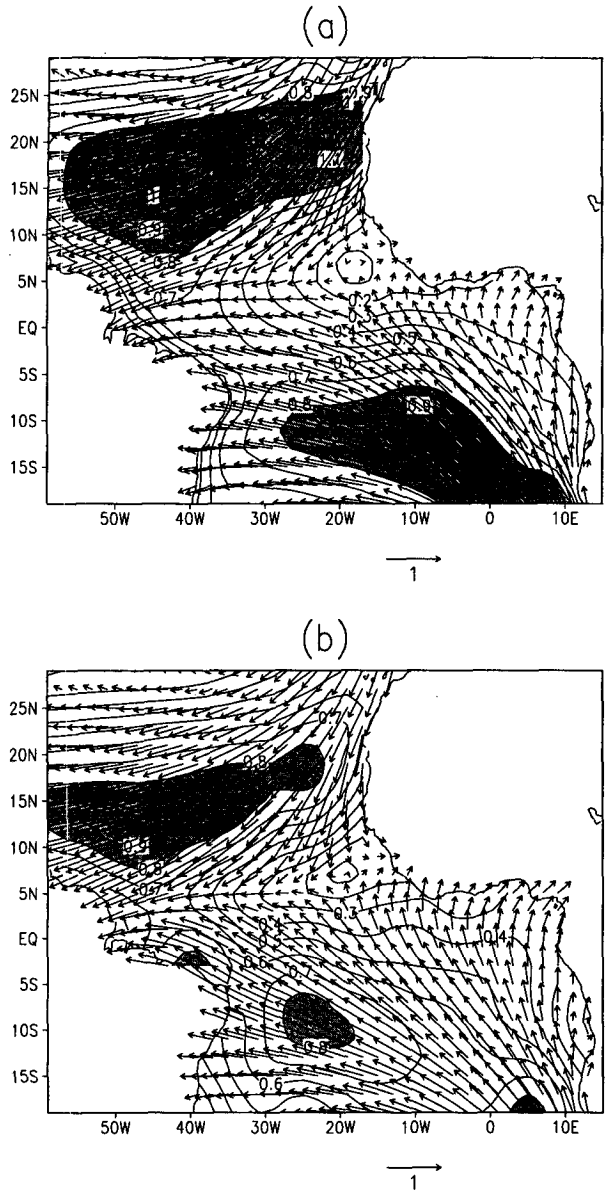

FIG. 1. Mean sea surface wind stress over tropical Atlantic Ocean for 1980–87. The arrow at bottom right corresponds to 1 dyn cm^{-2}. Contours of the stress magnitude are superimposed on the vectors with interval of 0.1 dyn cm^{-2}. Regions with the magnitude higher than 0.8 dyn cm^{-2} are shaded. The upper panel (a) is for the E-winds and the lower panel (b) for the S-winds.

1b). The E-winds (Fig. 1a), however, are more zonally oriented within 5°S–5°N and the ITCZ is hard to distinguish. These differences may reflect the fact that the ECMWF assimilation system tends to underestimate the divergent component of the wind field in low latitudes during this period. Trenberth et al. (1989b) have shown that the ECMWF monthly mean wind convergence near the equator fails to agree with that expected from satellite observed outgoing longwave radiation.

Several factors may contribute to the larger magnitude of trade winds in the E-winds data. First, the 1000-mb wind used in calculating the E-winds may overestimate the surface wind in the subtropics. It is also possible that the criteria of wind quality check in calculating S-winds may cause a systematic underestimation of the monthly data. Observations with wind speed higher than 25 m s^{-1}, such as those in tropical cyclones, were eliminated before calculating the monthly pseudo-wind stress (Servain et al. 1987). Lesser samples used to construct the S-winds may also cause an underestimate of its mean magnitude. This is because the surface wind stress as defined by (1) is the product of winds so that it is contributed by both the mean and the variance of the winds. As such, more data are apt to increase its magnitudes, especially in regions where transient effects are significant. We then expect that the magnitude of trade wind stress is somewhere between the two estimates.

The strongest variation of the surface wind stress over the tropical Atlantic Ocean is its annual cycle. The main features of the annual cycle can be seen from the monthly climatological mean wind stress in January, April, July, and October of the S-winds (Fig. 3). The most distinguishing feature is the migration of the ITCZ between the equator and 10°N, which is closest to the equator in boreal spring (Fig. 3b) and farthest north in late boreal summer and early fall (Fig. 3d). Each of the trade wind systems also undergoes an annual cycle of equatorward migration and zonal expansion into the western oceans during winter and spring of its hemisphere, followed by poleward migration and contraction into the central and eastern oceans during the summer and fall of its hemisphere.

The differences between the E-winds and the S-winds during these months are shown in Fig. 4. Over the tropical north Atlantic Ocean, the most persistent difference is the residual northeasterly wind stress to the north of 15°N throughout the year, which is strongest in the boreal winter (Fig. 4a) and weakest in fall (Fig. 4d). On the other hand, a residual southeasterly wind stress appears in central and eastern part of the tropical southern Atlantic Ocean, which is strong in the austral winter–spring (Figs. 4c,d) and weak in austral summer–fall (Figs. 4a,b). Both features reflect stronger trades of the E-winds, especially in the winter hemisphere. Another pronounced feature in the difference maps is a pattern of residual meridional divergence over the equatorial ocean, which follows the annual migration of the ITCZ.

We further discuss the implications of different mean wind stresses in forcing the large-scale ocean circulation using the mean monthly SST and upper-ocean heat content (HC) from the OGCM simulations, respectively, forced by these two wind stresses. The HC is defined as the mean temperature averaged for the depth of upper 317 m in the ocean domain. In general, the HC is an approximate measure of the thermocline

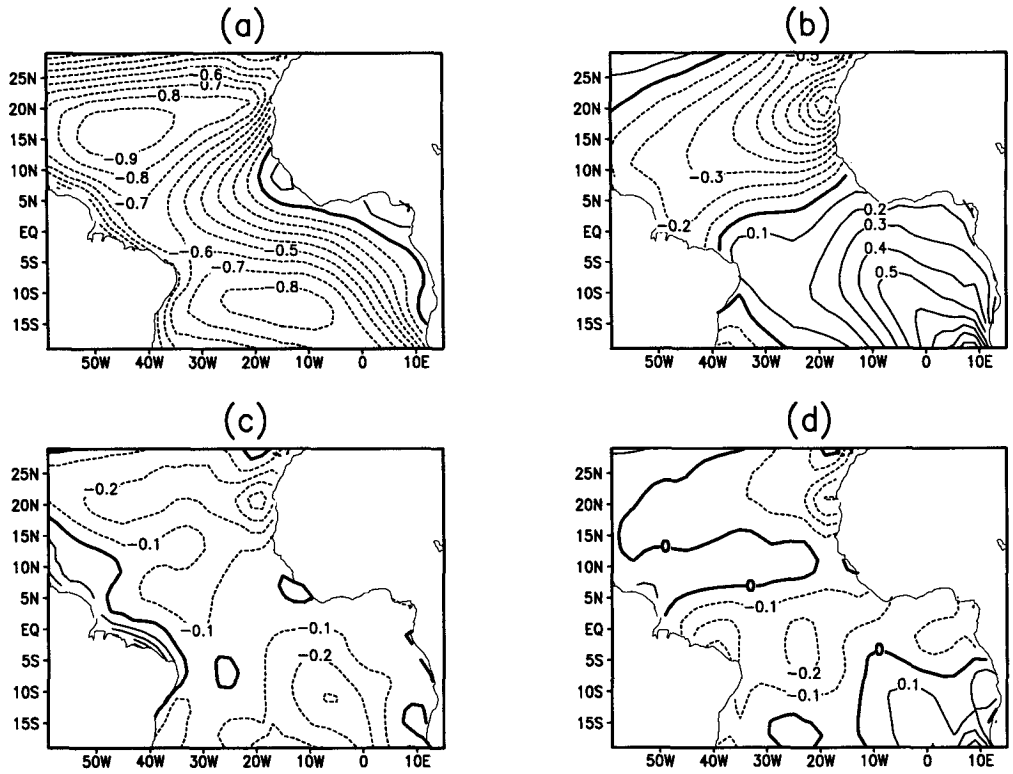

FIG. 2. Mean wind stress components and the difference between two datasets over the tropical Atlantic Ocean in 1980–87 for (a) τ_x for E-winds, (b) τ_y for E-winds, (c) τ_x difference for E-winds minus S-winds, and (d) τ_y difference for E-winds minus S-winds. The contour intervals are 0.1 dyn cm^{-2} for all panels.

depth, sea level, and the dynamic height (Rebert et al. 1985). In the Tropics, its annual cycle is mainly caused by vertical movements of the thermocline associated with the dynamical response of the ocean to the seasonally varying winds. Merle (1980) found that the seasonal HC variations are about ten times larger than the seasonal variations of the heat gain from the atmosphere through the surface in the equatorial Atlantic Ocean.

First, the simulated SST and HC mean fields are verified by comparing them with their corresponding observations. The observed climatological monthly SST and HC are derived from the observed ocean climatological temperatures, constructed by Levitus (1982) based on monthly objective analyses on a composite of station data, expendable bathythermograph (XBT) data, and mechanical bathythermograph data on file at the National Oceanographic Data Center. The original data are global on a 1° × 1° grid on chosen vertical levels with intervals increasing from 10 m at the sea surface to 50 m at the depth of 300 m. The temperatures are interpolated to the model grid point before integrated into HC.

As expected, the mean SSTs from these two runs are close to each other (Figs. 5a,b) and are qualitatively similar to the observed climatological SST (Fig. 5c). Quantitatively, the simulated mean SSTs are about 1°–1.5°C colder than the observations in the equatorial region but 1°–1.5°C warmer in the subtropics, as well as on the northern coast of the Gulf of Guinea. The mean SST of the S-winds simulation is warmer than that of the E-winds simulation in most of the domain because the surface winds modulating the evaporative and sensible heat fluxes are weaker in the S-winds.

The mean HC states from both simulations are also qualitatively similar to each other. As an example, the HC pattern from the S-winds simulation is given in Fig. 6a. In general, it shows alternating highs and lows in the meridional direction. Superimposed on the meridional structure are gradients in the zonal direction extending from lower values in the east and higher values in the west for most of the tropical ocean. Off the equator, the zonally directed ridges and troughs are associated with oceanic currents through geostrophic balance. For example, the North Equatorial Counter Current (NECC) flows eastward within 3°–10°N, between the ridge around 3°N and the trough at about 10°N. Farther north, there is the westward flowing North Equatorial Current. Close to the equator, the currents tends to follow the pressure gradient because the Coriolis force vanishes.

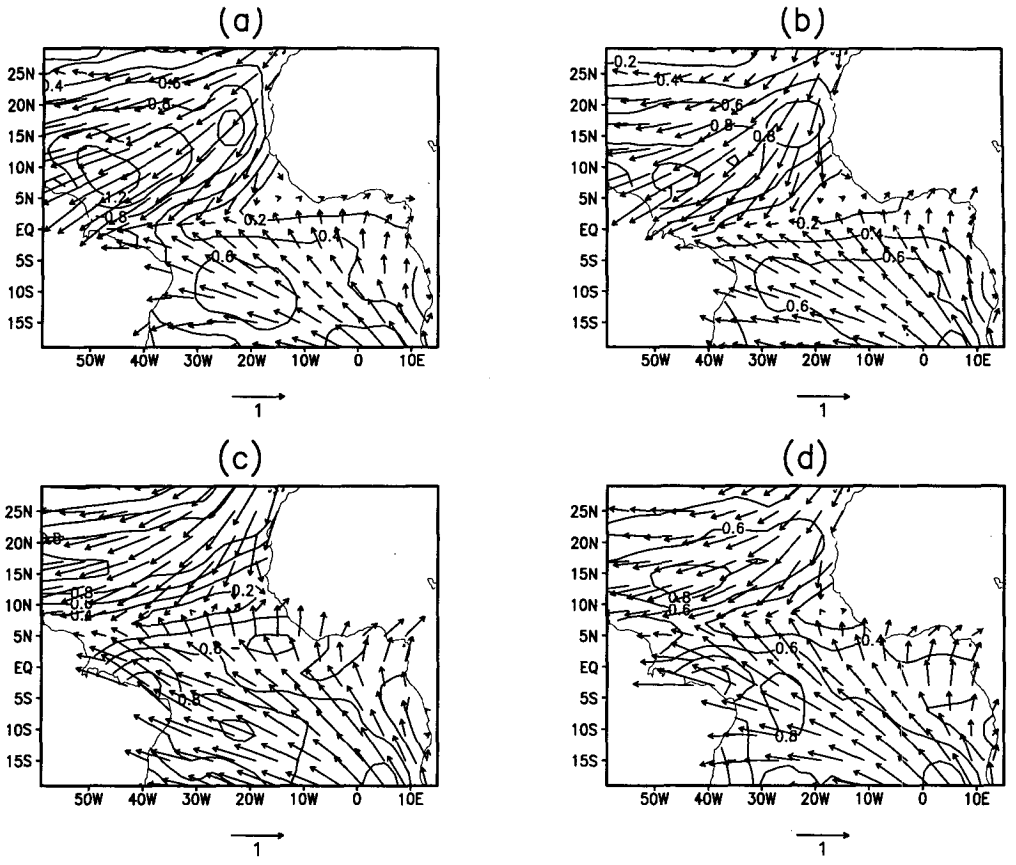

FIG. 3. Mean monthly sea surface wind stress over tropical Atlantic Ocean from the S-winds for (a) January, (b) April, (c) July, and (d) October. The arrow at bottom right corresponds to 1 dyn cm^{-2}. Contours of the stress magnitude are superimposed on the vectors with interval of 0.2 dyn cm^{-2}.

The quantitative difference of the mean HCs from these two simulations is shown in Fig. 6b. The mean temperature from the S-winds simulation is higher in most of the domain. The warmest region is around the eastern coast and in the Gulf of Guinea. Part of the reason for warmer mean temperature in the S-winds simulation is related to its reduced heat loss at the sea surface, which also causes warmer SST. The weaker zonal S-winds also lead to a flatter thermocline slope around the equator and deeper thermocline depth in the eastern equatorial ocean.

There are two regions where the mean temperature from the E-winds simulation is warmer. One is the western and central part of the tropical southern Atlantic Ocean centered at 10°–15°S with maximum temperature difference 0.5°C. This difference is apparently related to the eastward shift of the maximum southeast trades of the E-winds in comparison with the S-winds. The other is in the equatorial and tropical north Atlantic Ocean to the west of 30°W between 5° and 10°N. This reflects the fact that the zonal trough originating in the eastern ocean at 10°N does not extend as far west in the E-winds simulation as in the S-winds simulation. The excessive warm water pushed poleward from the western equatorial ocean by stronger mean equatorial zonal E-winds through Ekman pumping may be a reason for warmer off equatorial water in the western Atlantic in the E-winds simulation.

The differences between the simulated mean HC states and the observations (i.e., the systematic errors of the simulated HCs, Figs. 6c,d) are larger than the HC difference between the two simulations (Fig. 6b). The patterns of the systematic errors from both runs are qualitatively similar. The simulated upper oceans are about 1°–2°C colder than the observations in the zonal belt between 10° and 25°N, which are associated with the weaker ridges at 20°N in both simulations. Similarly, the simulated ridge around 15°S is also weaker than the observed one, so that there are negative errors in the western part of the tropical south Atlantic Ocean. On the other hand, the simulated upper ocean is warmer than observations within 10°S–10°N.

It seems that the main features of the systematic HC errors of the OGCM, that is, the cooling in the north and warming in the equatorial ocean, are not sensitive to the difference in surface wind forcings except near

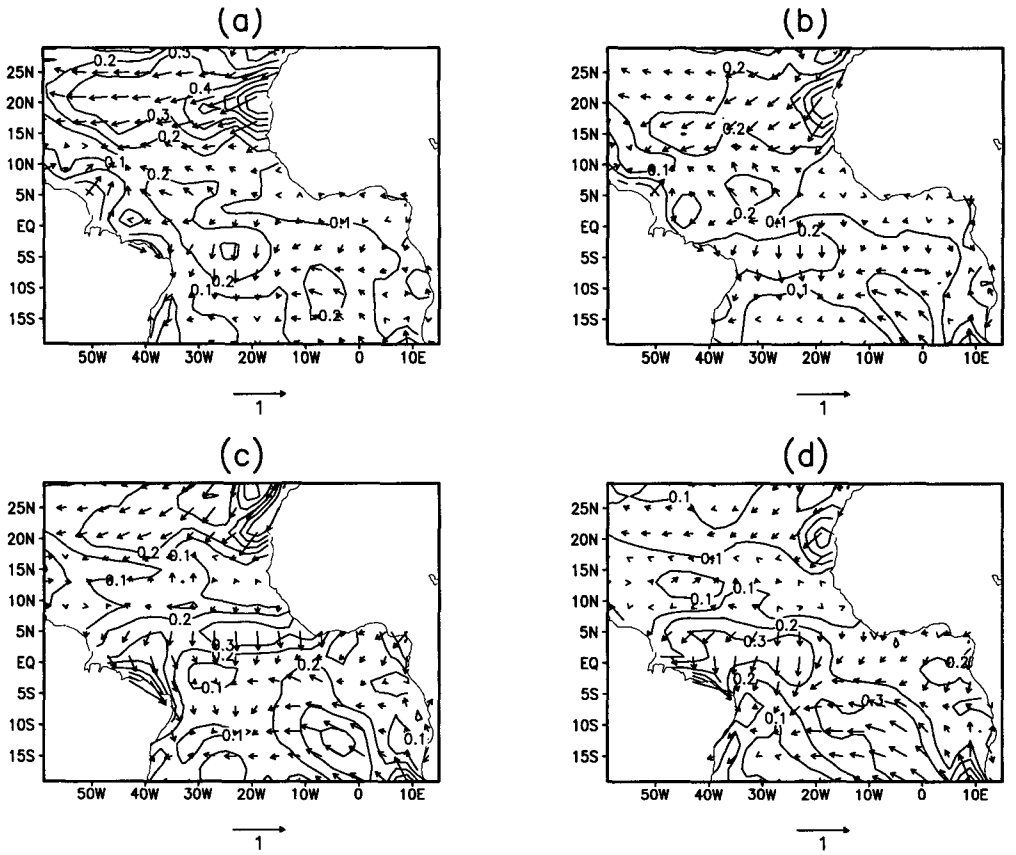

FIG. 4. The difference of mean monthly sea surface wind stress over tropical Atlantic Ocean between the E-winds and the S-winds for (a) January, (b) April, (c) July, and (d) October. The arrow at bottom right corresponds to 1 dyn cm^{-2}. Contours of the stress magnitude are superimposed on the vectors with interval of 0.1 dyn cm^{-2}.

the eastern coast, where the positive errors are reduced significantly when the E-winds are used to force the model. It is also unlikely that these errors are caused by the heat flux parameterization because the mean SSTs, which are directly affected by the surface heat fluxes, show errors that are nearly opposite to those of the HCs, with colder equatorial ocean and warmer subtropics. These errors could be explained as the effect of inadequate meridional heat transport within the ocean.

The largest annual changes of the mean temperature (or the thermocline depth) occur between 10°S and 10°N, in association with the fluctuations of the ridge to the north of the equator (3°–5°N) and the trough to the south (0°–3°S), as seen from the monthly data of the S-winds simulation in January, April, July, and October (Fig. 7). As a result, the zonal gradient along the equator is steeper in boreal summer and fall (Figs. 7c,d) but flatter in boreal winter and spring (Figs. 7a,b). The differences of the mean temperatures between the S-winds and E-winds simulations, as seen from the annual means, also appear seasonally (Fig. 8). The deeper thermocline in the E-winds simulation in the western equatorial ocean is more significant in the boreal fall and winter, as is the shallower thermocline in the Gulf of Guinea (Figs. 8a,d). The differences in the tropical south Atlantic Ocean are similar throughout the year.

4. Interannual variability

In this section, we examine the interannual variability of the surface wind stress over the tropical Atlantic Ocean during 1980–1987 as revealed from these two datasets. The interannual signals are studied using monthly anomaly data, defined as differences between the monthly mean fields and the corresponding monthly climatology. The major interannual modes of the surface wind stress are extracted using statistical methods. The common features and differences of both datasets are discussed. The sensitivity of the interannual signals simulated by the two OGCM experiments to the difference of the surface wind forcings is also examined.

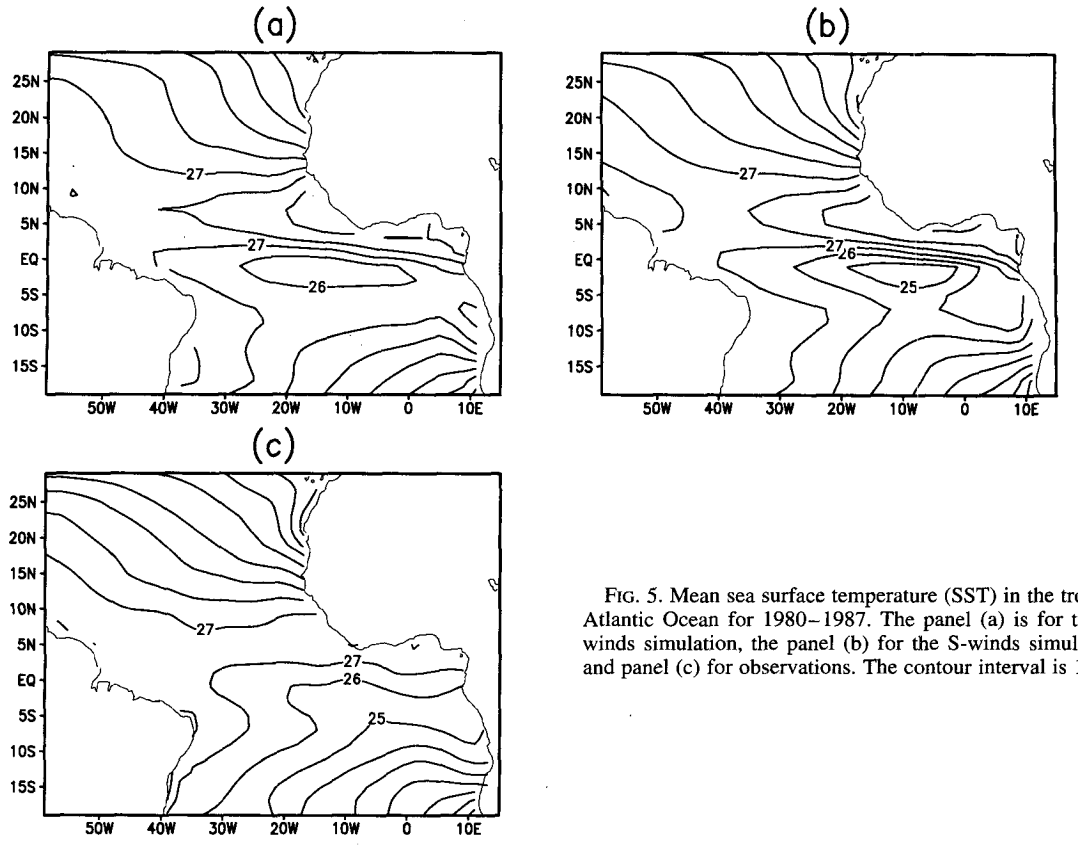

FIG. 5. Mean sea surface temperature (SST) in the tropical Atlantic Ocean for 1980–1987. The panel (a) is for the E-winds simulation, the panel (b) for the S-winds simulation, and panel (c) for observations. The contour interval is 1°C.

a. Statistical analysis

The methods of the empirical orthogonal function (EOF) and the singular value decomposition (SVD) are used to analyze the major interannual modes from the two sets of surface wind stress. The EOF extracts spatial–temporal orthogonal modes from a dataset that accounts for maximum possible variance (e.g., Kutzbach 1967). On the other hand, the SVD identifies pairs of modes that explain the maximum possible mean squared temporal covariance (see, e.g., Prohaska 1976; Lanzante 1984; Bretherton et al. 1992; Wallace et al. 1992). Therefore, the former is useful in deriving dominant signals from a dataset and the latter in getting signals from two datasets that are closely correlated with each other.

The EOF and SVD modes are derived for zonal and meridional components of the surface wind stress separately using data in the Atlantic Ocean within 20°S–20°N. Since the contribution of each EOF or SVD mode to the original data equals to the multiplication of its spatial pattern (the EOF or SVD pattern) and time coefficient (the principal component or SVD time series), we can normalize the time coefficient by its maximum within the whole period and times the spatial pattern with the same value to keep their multiplication unchanged. This procedure makes the absolute value at any given point of the spatial pattern representing the local amplitude of this mode.

The leading EOF modes derived from each dataset separately are very similar to the leading SVD modes derived with both datasets combined together. This is especially true for the zonal wind stress anomalies where the first EOF modes and SVD modes are actually indistinguishable. It is encouraging to find that the major interannual signals in both datasets are temporally consistent. In following discussion, we mainly present the modes derived from SVD analysis. Some relevant results of the EOF analysis are also discussed in order to substantiate the argument that the SVD modes do represent the major signals of the datasets.

The first SVD mode of the anomalous zonal wind stress τ_x explains about 37% of the total cross-covariance, as well as 38% and 21% of the E-winds and S-winds variances. The spatial patterns from the two datasets are quite similar (Figs. 9a,b), both are dominated by easterly anomalies north of the mean ITCZ. To the south, there are weak westerly anomalies in the western equatorial ocean that extend southeastward into the tropical south Atlantic Ocean. Quantitatively, the magnitude of the easterly anomalies in the E-winds is about two times the S-winds over the northernmost latitudes. The E-winds westerly anomalies

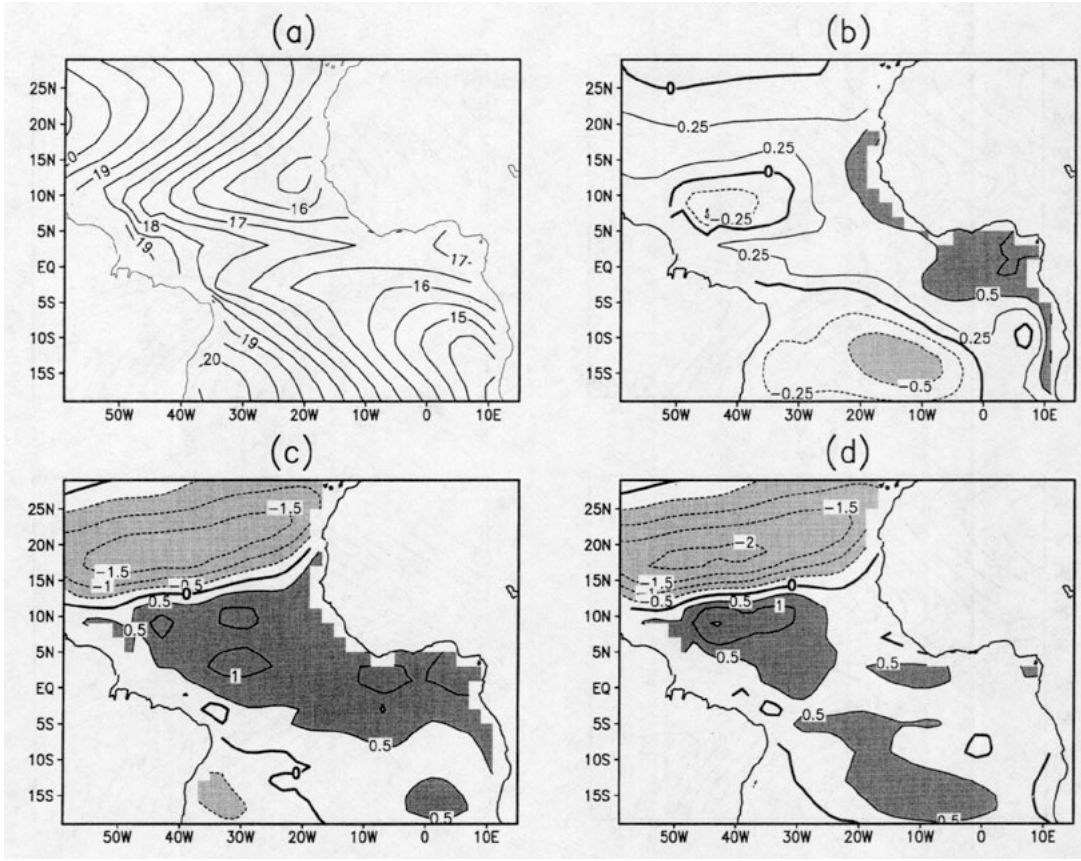

FIG. 6. (a) The mean upper ocean heat content (HC) of the tropical Atlantic Ocean from the S-winds simulation. The contour interval is 0.5°C. (b) The mean HC difference between the S-winds and the E-winds simulations. (c) The mean HC error by the S-winds simulation. (d) The mean HC error by the E-winds simulation. The contour interval is 0.5°C in (c) and (d) and 0.25°C in (b). In (b), (c), and (d), regions with temperature difference greater than 0.5°C have dark shading and regions with temperature difference less than −0.5°C have light shading.

are also higher in the eastern part of the tropical south Atlantic Ocean.

The two SVD time series (Fig. 9c) are highly correlated with each other (correlation coefficient 0.90). The most prominent feature of these series is a positive tendency from 1980/86 so that both curves develop from negatives during 1980/81 to positive during 1984–86. Superimposed on this apparent trend are "anomalous events" on monthly and seasonal timescales, such as the positive peaks in the boreal winter of 1981/82, 1983/84, 1984/85 and 1985/86; and the negative peaks in 1982/83 and 1986/87. There is also close agreement between the two curves on these higher frequency features.

The first SVD patterns of τ_y (Figs. 10a,b) characterizes anomalous north wind over the tropical north Atlantic Ocean. The center of anomalies is located in the central part of the ocean for the E-winds but closer to the Senegal coast for the S-winds. A secondary center of the northerly anomalies is over the western equatorial ocean with the S-winds stronger. There are also northerly anomalies in the southeast part of the ocean. This mode explains 23% of the total cross-covariance as well as 20% and 18% of the E-winds and the S-winds variances, respectively.

The two SVD time series of the first SVD mode of the anomalous meridional wind stress τ_y show close in-phase fluctuations (correlation coefficient 0.86). Moreover, the τ_y and τ_x time series for the first SVD modes (Figs. 9c, 10c) are also highly correlated (with correlation coefficients as high as 0.83 between the E-winds patterns and 0.70 between the S-winds patterns). The in-phase fluctuations of the τ_x and τ_y modes of the first SVDs, shown in both datasets, suggest that they describe the same wind stress fluctuation.

The second SVD mode of τ_x (Figs. 11a,b) accounts for 11% of the total covariance and 18% and 9% of the E-winds and S-winds variances, respectively. Both spatial patterns show the easterly anomalies extending northwestward from the south along the Brazilian coast across the equator. In detail, there are significant differences between the patterns from the two datasets. The easterly anomalies from the S-winds are centered at about 10°S, 25°W with magnitude of 0.25

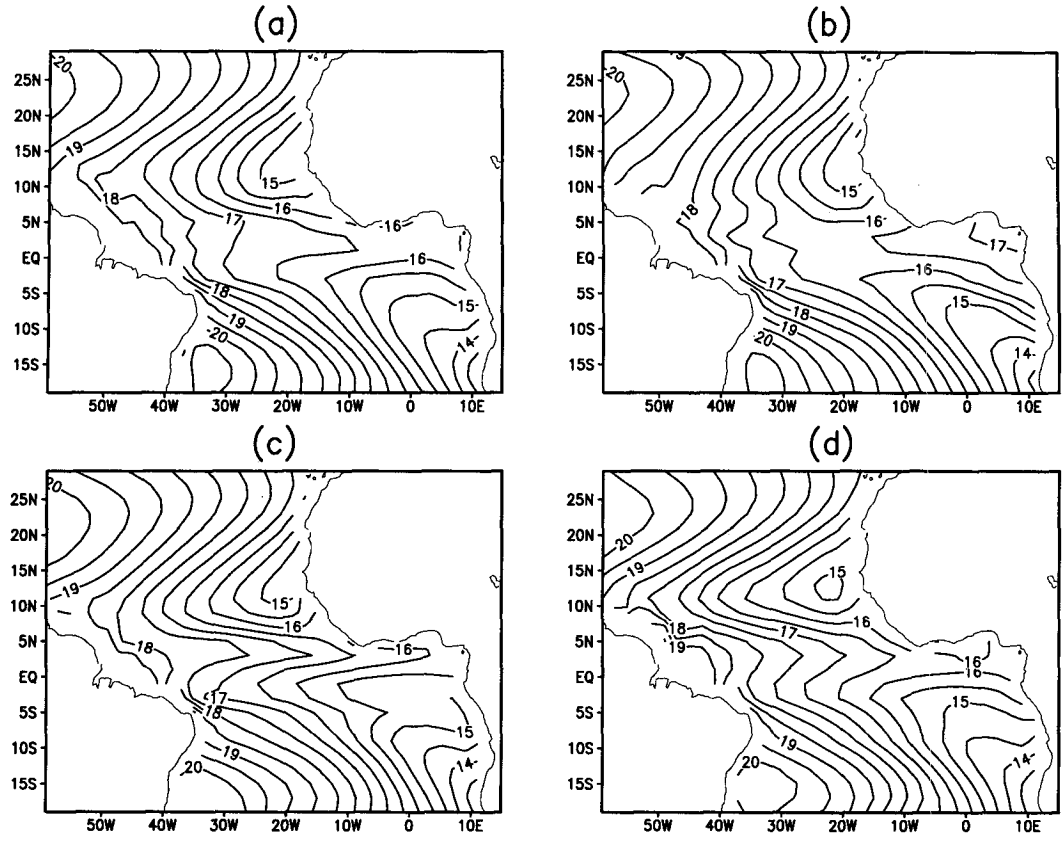

FIG. 7. Mean monthly HC fields from the S-winds simulation for (a) January, (b) April, (c) July, and (d) October. The contour interval is 0.5°C.

dyn cm^{-2}. There are no significant anomalies to the east of 10°W in the south. The anomalies in the E-winds, on the other hand, have their maximum much farther south and have larger amplitude (0.4 dyn cm^{-2}). Moreover, the anomalies extend both northwestward across the equator and toward the east so that the ocean to the south of the equator and west of 5°W is covered with anomalies with 0.2 dyn cm^{-2}.

The correlation coefficient of the two time series for the second SVD mode is 0.59. Both time series are generally positive during 1981–83 and negative during 1984–86 (Fig. 11c). The fluctuations of the E-winds in this period look like a negative trend, starting from positive in 1981 and gradually reducing to negative in 1984. However, the positive values in the S-winds are maintained from 1981 to 1983, abruptly changing to large negative in 1984. The two curves significantly deviate from each other during 1980–81. The E-winds show large negative in 1980 and large positive in 1981. The S-winds, on the other hand, are not far from zero in both years.

The second mode of τ_y explains 11% of the total covariance and 12% and 8% of the E-winds and S-winds variances. This mode describes an out of phase fluctuations between the equatorial ocean centered at the Brazilian coast and the eastern part of the tropical North Atlantic Ocean near the Senegal coast (Figs. 12a,b). As with the second mode of τ_x, the differences between the patterns from the two datasets are in the eastern ocean, where the E-winds show larger anomalies. The correlation coefficient of the SVD time series is relatively high (0.79). Moreover, their behavior (Fig. 12c) have some similarity with those of the second mode of τ_x (Fig. 11c), with positive values in 1981–83 and negative values in 1984–85.

As shown above, the first or second modes of the τ_x and τ_y can be combined because they describe the two components of the same wind stress fluctuations. Moreover, the first SVD mode mainly describes wind stress anomalies to the north of the equator, corresponding to the fluctuations of the northeast trades. The second SVD modes of τ_x and τ_y, to a lesser extent, may also be combined to characterize fluctuations in the south and near the equator, corresponding to the fluctuations of the southeast trades, which are negatively correlated with wind fluctuations over the eastern part of the tropical north Atlantic.

Therefore, as a synthesis of the first two SVD modes of both wind components, the low-frequency variation of the tropical Atlantic wind stress during 1980–87

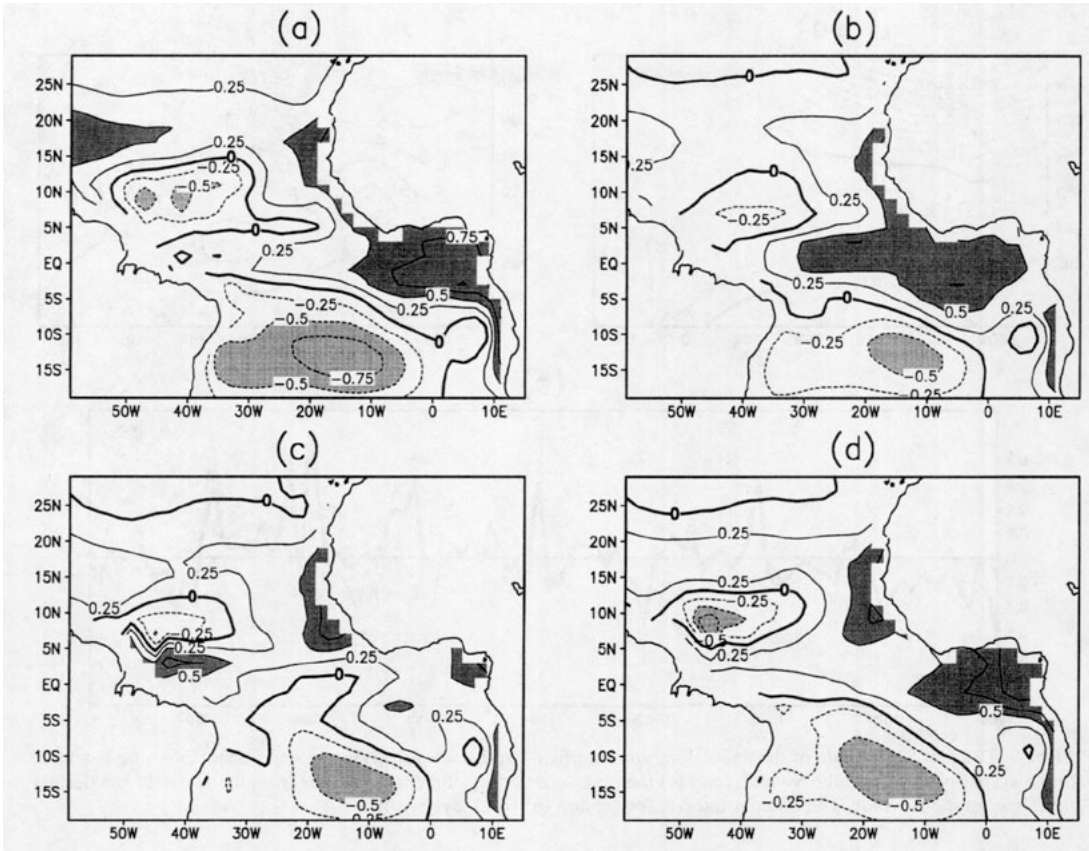

FIG. 8. The difference of the mean monthly HC fields between the S-winds and the E-winds simulations for (a) January, (b) April, (c) July, and (d) October. The contour interval is 0.25°C. Regions with temperature difference greater than 0.5°C have dark shading and regions with temperature difference less than −0.5°C have light shading.

from both datasets can be summarized as follows. The northeast trade winds were generally increasing from 1980 to 1986, which were weaker than the climatology from 1980 to 1983 but stronger from 1984 to 1986. On the other hand, the southeast trade winds are stronger than the climatology from 1981 to 1983 but weaker from 1984 to 1985. This decrease of the southeast trades from 1981–86 were gradual in the E-winds. Therefore, a dominant interannual signal in the surface wind stress over the tropical Atlantic Ocean is an alternate strengthening and decaying of the two trade wind systems. Superimposed on these low-frequency changes were fluctuations with timescales of several months.

The two leading SVD modes together explain about 48% (37% + 11%) for zonal and 34% (23% + 11%) for meridional components of the cross covariance between the E-winds and S-winds. So it is reasonable to say that these modes represent the major common variations in the two datasets. However, the dominance of these modes within their corresponding datasets is different. For instance, although the percentages of variances explained by the SVD modes of the meridional wind stress are comparable between the two datasets, they are very different for the zonal component. In fact, there are 56% (38% + 18%) for the zonal E-winds but only 30% (21% + 9%) for the zonal S-winds variances explained by the two leading SVD modes. Since the calculation gives each field the same weight by using the same number of grid points from each dataset, this difference should not come from bias of analysis. It actually suggests that the signals picked up by the leading SVD modes in the S-winds is much weaker than the corresponding signals in the E-winds.

The EOF analyses done separately for each dataset give similar results. The two leading EOF modes of the zonal component of the E-winds explains about 59% (39% + 20%) of the total variance, but those of the S-winds only explain about 33% (22% + 11%) of its total variances. This is approximately the percentages explained by the SVD modes because, as we have mentioned before, the SVD and EOF modes are quite similar to each other. Moreover, the first ten EOF modes of the E-winds and the S-winds account for 90% and 70% of the variances, respectively. It is clear that the distributions of variance in temporal and spatial scales are different within the two datasets. Much more variances are in smaller scales of space or time for the S-winds than for the E-winds.

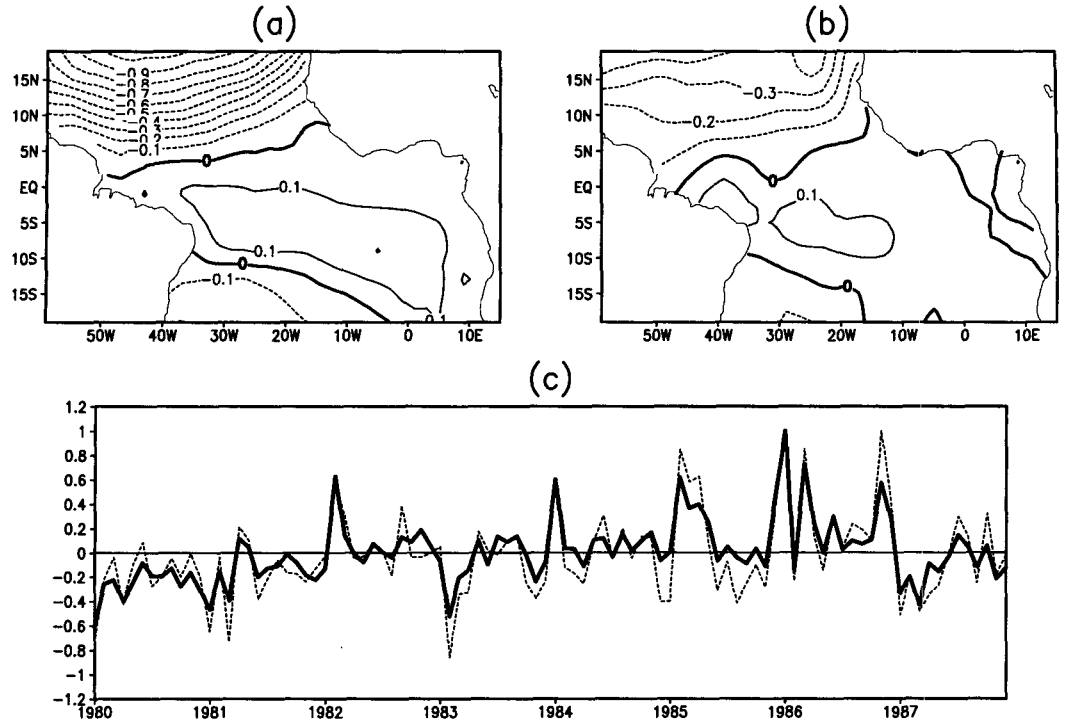

FIG. 9. The first SVD mode of the anomalous zonal surface wind stress for (a) the spatial pattern from the E-winds, (b) the spatial pattern from the S-winds, and (c) the time series. The solid curve in (c) is from the E-winds, the dashed curve is from the S-winds. The contour interval for (a) and (b) is 0.1 dynes cm^{-2}.

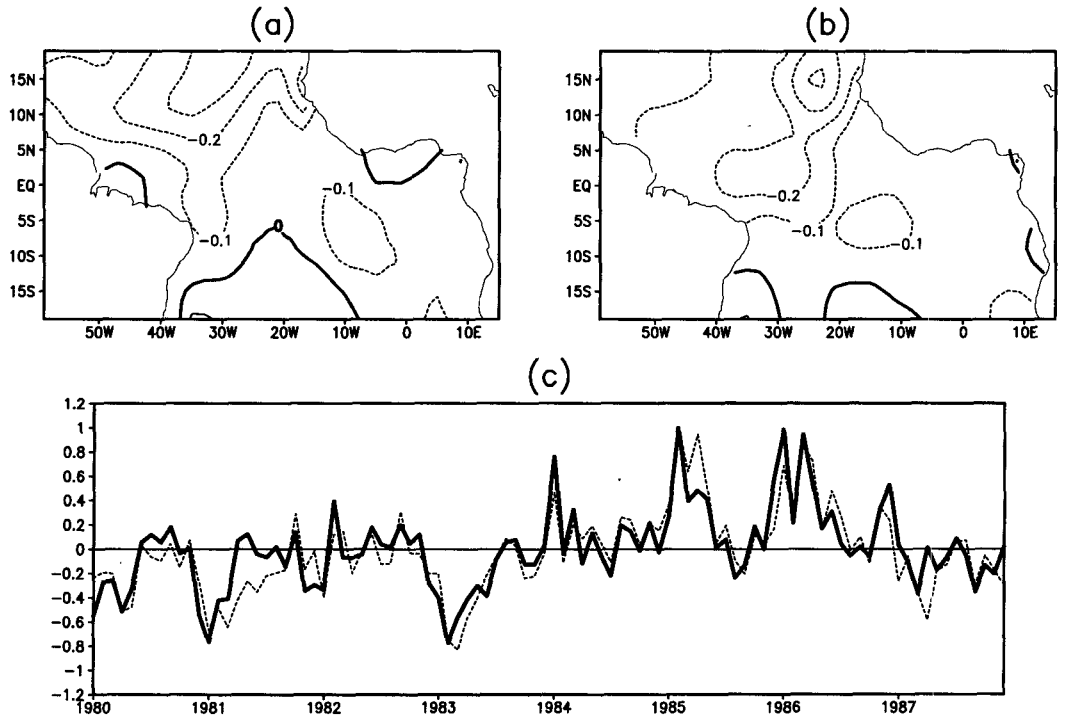

FIG. 10. The first SVD mode of the anomalous meridional surface wind stress for (a) the spatial pattern from the E-winds, (b) the spatial pattern from the S-winds, and (c) the time series. The solid curve in (c) is from the E-winds, the dashed curve is from the S-winds. The contour interval for (a) and (b) is 0.1 dynes cm^{-2}.

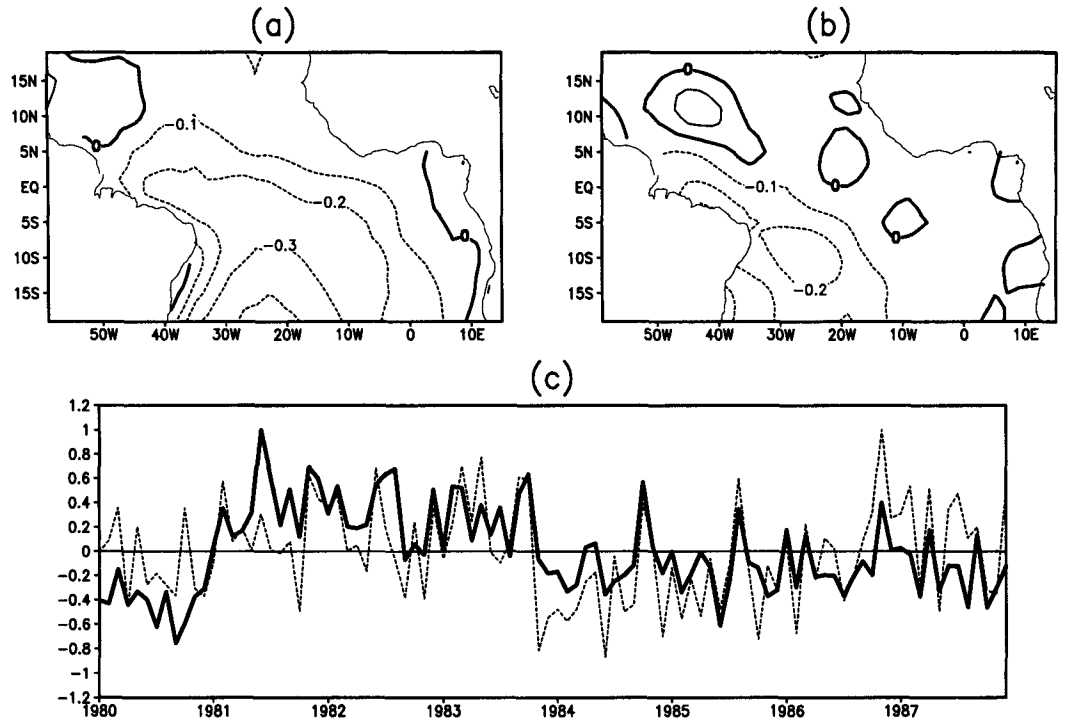

FIG. 11. The second SVD mode of the anomalous zonal surface wind stress for (a) the spatial pattern from the E-winds, (b) the spatial pattern from the S-winds, and (c) the time series. The solid curve in (c) is from the E-winds, the dashed curve is from the S-winds. The contour interval for (a) and (b) is 0.1 dyn cm^{-2}.

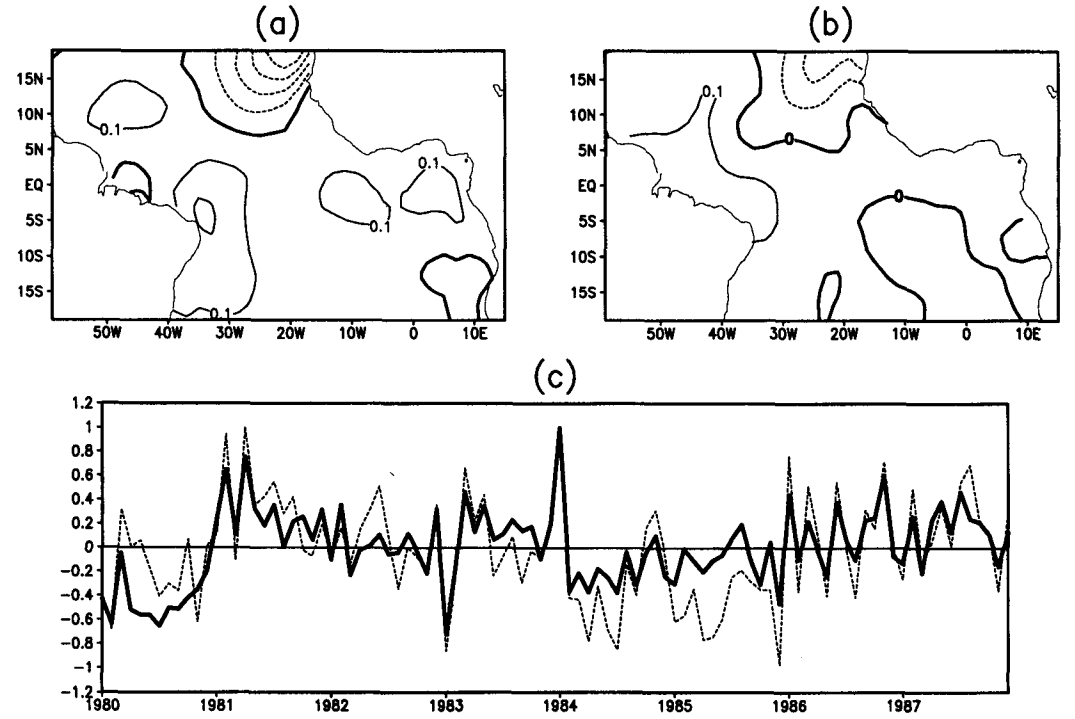

FIG. 12. The second SVD mode of the anomalous meridional surface wind stress for (a) the spatial pattern from the E-winds, (b) the spatial pattern from the S-winds, and (c) the time series. The solid curve in (c) is from the E-winds, the dashed curve is from the S-winds. The contour interval for (a) and (b) is 0.1 dynes cm^{-2}.

b. Model results

As in section 3, we examine the OGCM simulated interannual variability using the SST and HC anomalies from both experiments. Previous modeling studies have shown that the oceanic thermocline (or HC) responds realistically to interannual fluctuations of surface wind stress forcing in the tropical Atlantic Ocean (e.g., Reverdin et al. 1991; Huang 1992; Carton and Huang 1994; Huang et al. 1995). Moreover, Huang et al. (1995) showed that the fluctuations of the indices for interannual SST variations in the tropical Atlantic Ocean as defined by Servain (1991) can be reproduced qualitatively by the OGCM forced with the ECMWF surface wind stress. Here we examine how sensitive the simulated interannual signals to the difference in wind forcings. We also try to judge the quality of the two wind stress datasets by examining how well the interannual SST anomalies can be reproduced. The monthly SST observations during 1980–87 used for verification are from Servain et al. (1987).

Figures 13a,b shows correlation coefficients between the observed and simulated SST anomalies. Both simulations have the highest correlations with the observations in the tropical north Atlantic Ocean. It is also the region with the best agreement between the wind stress datasets. The highest correlation appears near the Senegal coast for the S-winds where the SST is mainly affected by the alongshore meridional wind stress (Fig. 13a), and the best scores are over the western ocean for the E-winds where local winds are more zonally oriented (Fig. 13b). In the south, the correlations of the E-winds simulation are generally higher. Near the Angola coast, the correlation coefficients are around 0.4 for the E-winds simulation but generally less than 0.2 for the S-winds simulation. Along the equator, the correlations are quite low in both cases. In particular, significant negative values appear within the Gulf of Guinea. The patterns of root-mean-square (rms) errors for simulated SST anomalies from both runs are similar (Figs. 13c,d). In general, the rms errors are larger in the eastern coast and the equatorial ocean where SST fluctuations are significant. Therefore, it is hard to decide which forcing is better.

The correlations between the simulations and the observations are rather low in the equatorial Atlantic (10°S–10°N) in comparison with similar results derived from the Pacific Ocean where correlations between observed and simulated SST anomalies are highest near the equator (Miller et al. 1993). The difference between the two oceans may be due to the fact that the equatorial Pacific is dominated by strong interannual fluctuations associated with El Niño/Southern Oscillation events that account for most of the correlation, whereas the interannual signals in the tropical Atlantic are much weaker and have comparable magnitude to variations with shorter timescales of months. Since these higher-frequency fluctuations are not simulated adequately by the OGCM except in regions where observations are dense enough to pick up the corresponding wind signals accurately (such as in the tropical north Atlantic), it brings the correlation down.

Figures 14a,b shows the correlation and rms difference between the SST anomalies simulated by the two runs. It is interesting to note that the correlation in most of the equatorial and Southern Ocean is low, whereas it is significantly higher in the tropical north Atlantic Ocean. Also, the rms difference between the two runs is as large as the rms difference between either of them and the observations in the eastern coast and equatorial ocean (Figs. 13c,d). This suggests that the simulated SST anomalies by the OGCM are very sensitive to the difference of surface wind forcings.

Therefore, unlike the systematic errors of OGCM mean state and annual cycle that are not sensitive to differences of wind forcing, it seems that the accuracy of winds is essential to the simulation of SST anomalies in the tropical Atlantic Ocean. For instance, in the northern region where observations are plentiful and both datasets are closest to each other, the model gives the best simulations and the two runs are highly consistent with each other. However, in the equatorial and Southern Oceans, where observations are sparse and the two datasets show significant differences, the model behavior is poor and the consistency between the two simulations is low.

We further examine how well the basinwide low-frequency SST variations in the tropical Atlantic Ocean can be reproduced by the OGCM since the large-scale oceanic variations should be most closely related to the major interannual modes of the surface wind stress discussed above. This is done by projecting the simulated SST anomalies onto the leading modes of the empirical orthogonal functions (EOF) of the observed SST anomalies and measure how close the projection coefficients to the principal components of the observed modes.

Two leading modes are used to represent the basinwide fluctuations of observed SST anomalies. The first mode (Fig. 15a) shows anomalies with opposite signs occupying the Southern and the Northern Oceans, respectively, with the separation at 5°N. The largest anomalies are near the Angola coast. This mode explains 22% of the total variance. Its spatial structure is similar to the "dipole pattern" of the SST anomalies in the tropical Atlantic Ocean, discovered from extensive analyses of the observations (see, e.g., Lamb 1978a,b; Moura and Shukla 1981; Lamb et al. 1986; Servain 1991). The second mode (Fig. 16a), on the other hand, is of same sign over most of the basin and is dominated by anomalies extending from the Senegal coast into the open ocean. This mode explains about 17% of the total variance.

The projection of the simulated SST anomalies onto the first EOF mode is shown in Fig. 15b, together with the principal component from the observations. Start-

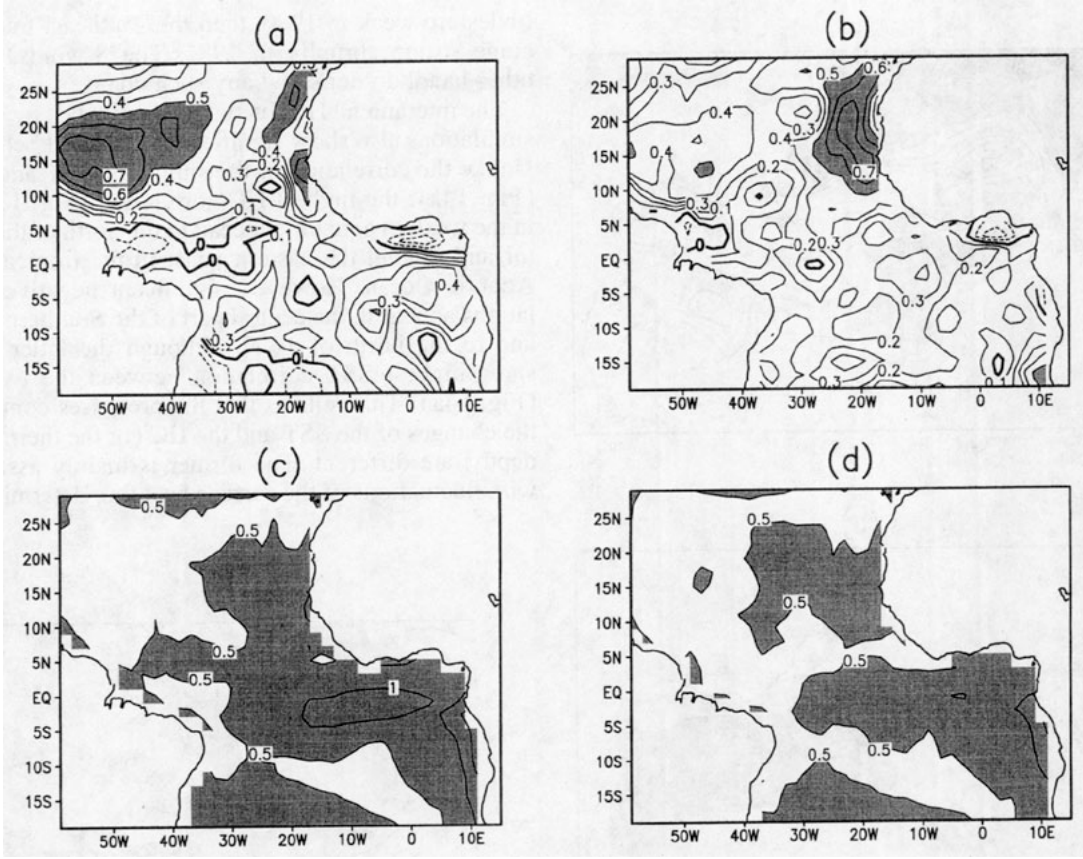

FIG. 13. Correlations and rms errors between the simulated and observed SST anomalies. (a) Correlation for the E-winds simulation, (b) correlation for the S-winds simulation, (c) rms error for E-wind simulation, and (d) rms error for the S-wind simulation. The contour interval is 0.1 with regions of correlation greater than 0.5 shaded for (a) and (b). For (c) and (d), the contour interval is 0.5°C with regions greater than 0.5°C shaded.

ing from negative values, the observations (heavy solid curve) shows a positive tendency in the first half of the period, with a gradual increase of the SST in the south and decrease in the north from 1980 to 1983. The largest positive values occurred in 1984 when a warm event started at the Angola coast, followed with a gradual decrease in 1985–86 and another increase at 1987.

Each simulation shows equally good consistency with the observations from 1984 to 1987 although the magnitude of the warm event in 1984 is underestimated by both of them. The correlation between the model projections and the observations is 0.56 for the E-winds and 0.48 for the S-winds simulation. On the other hand, the correlation between the two model projections is 0.45. By this measure, both projections are closer to the observations than to each other. The higher correlation coefficient for the E-winds simulation (the thin solid line) is mainly because it reproduces the observed positive tendency during 1981–83 for the first part of the period, whereas the S-winds simulation (the thin dashed line) shows no significant trend.

The time series of the simulated SST anomalies (Fig. 15b) and the τ_x and τ_y time series of the second SVD mode (Figs. 11c, 12c) have significant negative correlations. This suggests that this SST mode is closely related to the wind stress fluctuations as described by the second SVD mode. Warm (cold) SST anomalies appear near the equator and in the south when northwesterly (southeasterly) anomalies of the wind stress prevail there. Moreover, weaker opposite SST anomalies appear in the north simultaneously, possibly in response to anomalous meridional winds in the eastern part of the tropical north Atlantic Ocean.

The projections of the observed and simulated SST anomalies to the second EOF mode are shown in Fig. 16b. In this case, the correlations between the projections and the observations are 0.48 for the E-winds and 0.46 for the S-winds, and the correlation between simulations is 0.66. The simulations are close to each other from 1982 to 1987 and are consistent with the observations in the period 1983–86. Surprisingly, both simulations fail to reproduce the magnitude of the cold event in 1982 and the warm event in 1987. A common feature of all the curves in Fig. 16b is a negative tendency during 1980–86, showing a gradual cooling of the northern ocean. This is apparently related to the

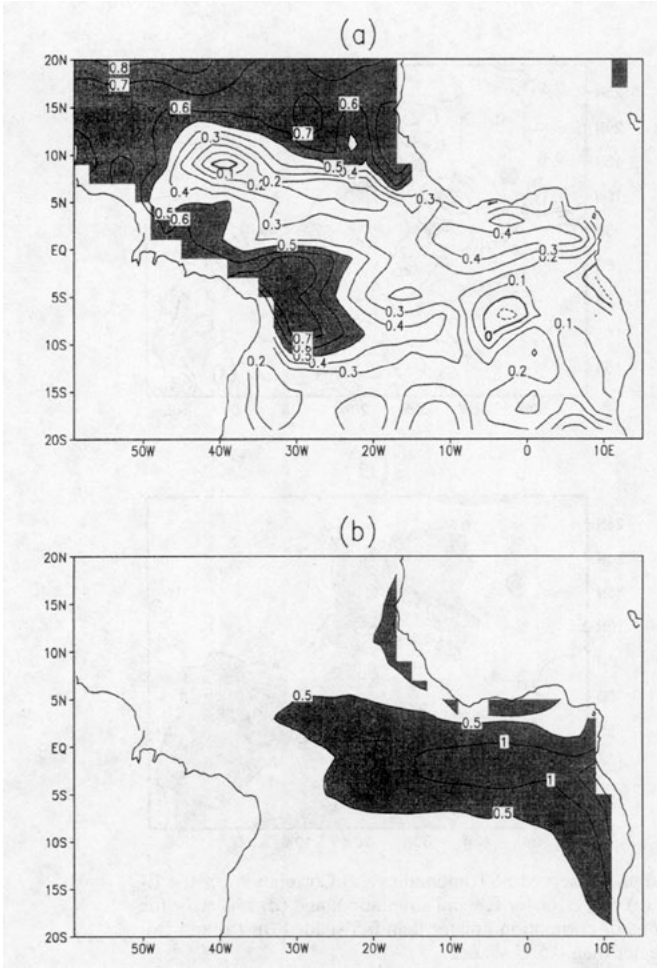

FIG. 14. Correlations (a) and rms difference (b) between the SST anomalies from the two simulations. The contour interval is 0.1 with regions of values greater than 0.5 shaded in (a). For (b), the contour interval is 0.5°C with regions greater than 0.5°C shaded.

tendencies of the surface wind stress described in the first SVD modes of τ_x and τ_y (Figs. 9, 10), showing a gradual strengthening of the northeast trade winds.

We notice that the differences are large between the two simulations in the first two years in the projections for both modes. A projection of the simulated SST onto the third EOF mode of the observations (not shown) also gives large discrepancies in 1981 between the two cases. This reflects fundamentally different variations produced by the two simulations during the period. In fact, the E-winds simulation produces basinwide warm SST anomalies in 1980, followed by strong cold anomalies near the eastern coast for both hemispheres, as well as around the equator in 1981. The S-winds simulation and the observations, on the other hand, show warm anomalies in late 1981. These discrepancies in the simulations are closely related to the differences of the wind stress anomalies between datasets. An examination of the E-winds in 1980–81 shows that both trades are weak in 1980, then the southeast trades become strong abruptly in 1981. The S-winds, on the other hand, do not show any such changes.

The interannual HC fluctuations produced by the two simulations also show significantly different behaviors. Unlike the correlation of the simulated SST anomalies (Fig. 14a), the highest HC correlation (Fig. 17a) are in the western equatorial ocean to the north of the equator and around the eastern coast in the tropical north Atlantic Ocean. However, significant negative correlations appear in the central part of the Southern Ocean and to the north of 10°N, although the latter region show highest SST correlation between the two runs (Fig. 14a). This reflects that the processes controlling the changes of the SST and the HC (or the thermocline depth) are different. The former is mainly associated with fluctuations of the surface heat flux determined by

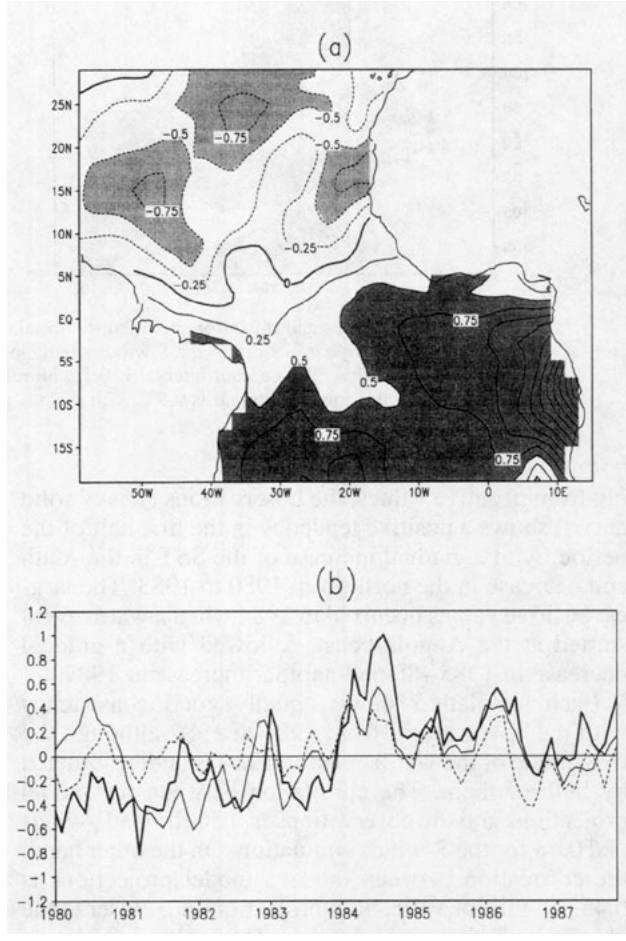

FIG. 15. (a) The first EOF mode of the observed SST anomalies during 1980–87 in the tropical Atlantic Ocean. (b) The projections of the observed and simulated SST anomalies to the first EOF mode of the observed SST anomalies. The heavy solid curve in (b) is from the observations, the thin solid curve is for the E-winds simulation, and the dashed curve is for the S-winds simulation. The contour interval for (a) is 0.25°C. Regions of SST anomalies greater than 0.5°C have dark shading and regions with SST anomalies less than −0.5°C have light shading.

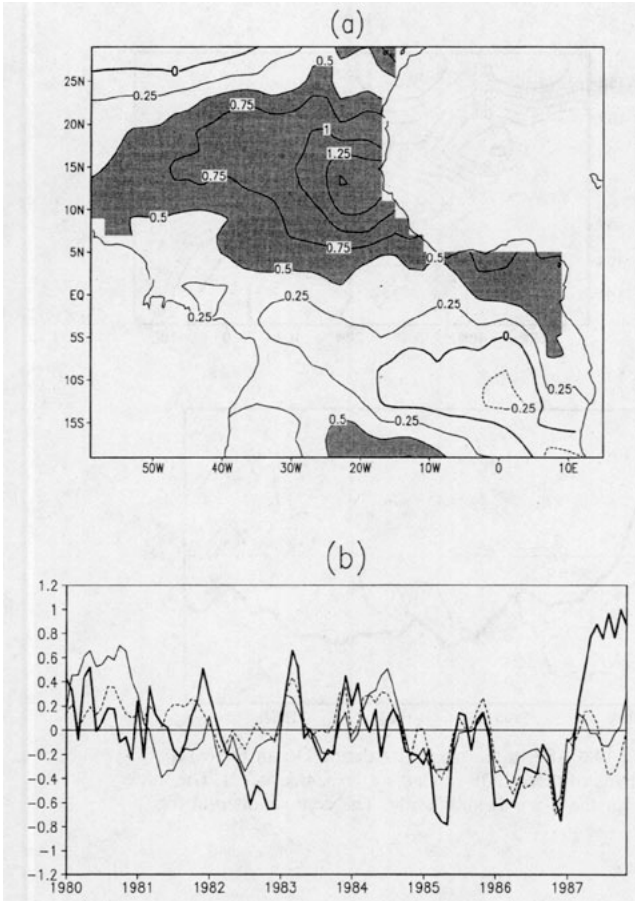

FIG. 16. (a) The second EOF mode of the observed SST anomalies during 1980–87 in the tropical Atlantic Ocean. (b) The projections of the observed and simulated SST anomalies to the second EOF mode of the observed SST anomalies. The heavy solid curve in (b) is from the observations, the thin solid curve is for the E-winds simulation, and the dashed curve is for the S-winds simulation. The contour interval for (a) is 0.25°C. Regions of SST anomalies greater than 0.5°C have dark shading and regions with SST anomalies less than −0.5°C have light shading.

the wind speed. The latter, however, are more strongly related to the changes in Ekman pumping produced by wind stress curls. The rms difference of the two HC anomalies (Fig. 17b) is largest in the western tropical Atlantic Ocean in both hemispheres, as well as around Angola coast where the HC variance is also the largest (Huang et al. 1995). The value of the difference is comparable to the amplitude of HC fluctuations there.

Figures 18 and 19 show the two leading EOF modes of the HC anomalies from both simulations. The corresponding modes from both data are presented together because they have clear resemblance in spatial structures. The first modes (Figs. 18a,b) shows opposite anomalies between the western and eastern part of the ocean. There are two major anomalies in the western ocean, which are located to the north and south of the equator and have opposite sign to the anomaly around the eastern coast to the south of the equator. Huang et al. (1995) pointed out that this HC pattern is associated with stronger than normal southeast but weaker northeast trades over the Atlantic Ocean. The second modes (Fig. 19a,b), on the other hand, show anomalies centered at the eastern equatorial ocean, which extends poleward along the eastern coast. This represents the displacement of the thermocline in response to the fluctuations of the zonal winds on the equator, in which perturbations of the thermocline generated by wind anomalies in the western ocean move eastward along the equator to the eastern coast then propagate poleward as coastal Kelvin waves (Moore et al. 1978; Serevain et al. 1982).

Though qualitatively similar, there are significant quantitative difference between the modes derived from different simulations. For the first EOF modes, the percentage of variance explained by the S-winds

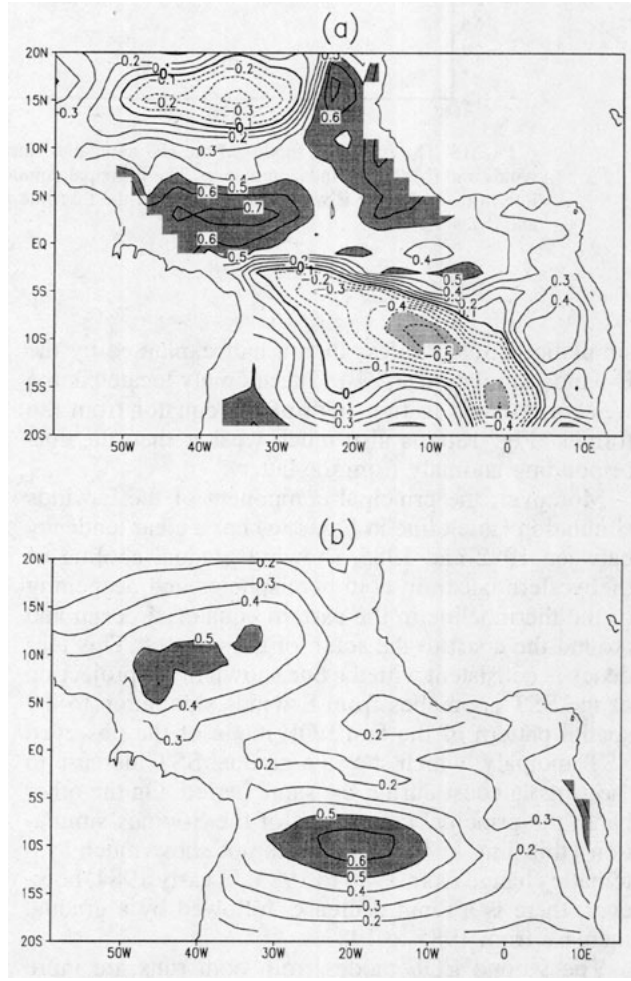

FIG. 17. Correlations (a) and rms difference (b) between the HC anomalies from the two simulations. The contour interval is 0.1 with regions of values greater than 0.5 darkly shaded and smaller than −0.5 lightly shaded in (a). For (b), the contour interval is 0.5°C with regions greater than 0.5°C shaded.

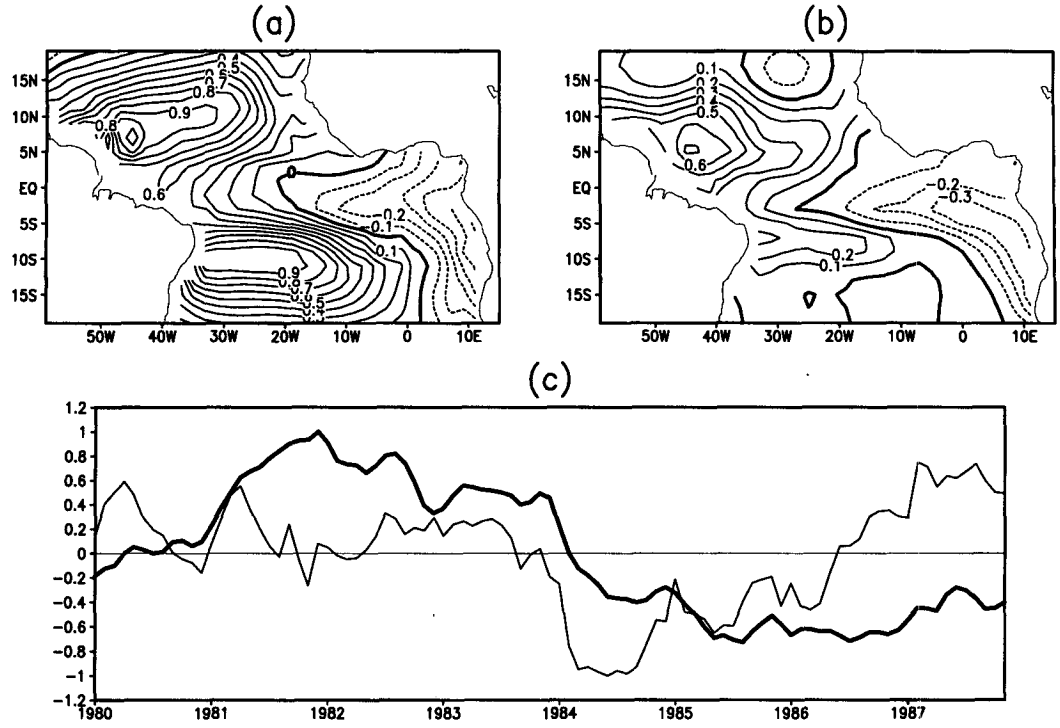

FIG. 18. The first EOF modes of the HC anomalies during 1980–87 in the tropical Atlantic Ocean for (a) the E-winds and (b) the S-winds simulation. The principal components of these EOF modes are presented in (c). The thick line in (c) is for the E-winds simulation and the thin line is for the S-winds simulation. The contour interval for (a) and (b) is 0.1°C.

simulation (30%) is less than a half explained by the E-winds simulation (63%). The anomaly located in the western Atlantic to the south of the equator from the former (Fig. 18b) is also much weaker than the corresponding anomaly from the latter.

Moreover, the principal component of the E-winds simulation (thick line in Fig. 18c) has a clear tendency between 1982 and 1985, showing gradual cooling of the western ocean in both hemispheres and deepening of the thermocline in the eastern equatorial ocean and around the coast to the south of the equator. This tendency is consistent with the one shown in the projection of the SST anomalies from E-winds simulation to the spatial pattern of the first EOF mode of the observed SST anomaly, which shows a gradual SST increase in the Angola coast during the same period. On the other hand, the principal component of the S-winds simulation (thin line in Fig. 18c) does not show much systematic change from 1980 to 1983. In early 1984, however, there is a rapid decrease, followed by a gradual increase from 1985 to 1987.

The second EOF modes from both runs are more consistent with each other. The percentages of variance explained are comparable (16% for the S-winds and 13% for the E-winds) and both show the warmings in 1984 and 1987 (Fig. 19c). The major difference is in 1980/81 when the E-winds simulation gives an intense cold event in the eastern ocean but the S-wind simulation shows a warm period. This discrepancy is clearly caused by the problems in the E-winds discussed above.

5. Summary

We have compared two monthly sea surface wind stress datasets over the tropical Atlantic Ocean during 1980–1987. These datasets are derived from two fundamentally different analysis schemes, one is the 1000-mb wind field based on the ECMWF operative analyses, the other is monthly pseudo-wind stress solely from ship observations.

Our examination shows that both datasets give qualitatively similar mean fields and annual cycles. The mean wind stress over the tropical Atlantic Ocean is composed of the northeast and southeast trade wind systems converging in the ITCZ north of the equator. The annual cycle is characterized by the intensification and equatorward extension of the northeast and southeast trade winds in boreal and austral winters, respectively, as well as the associated meridional ITCZ migration between the equator and 10°N. Quantitatively, the zonal component of the E-winds are larger than that

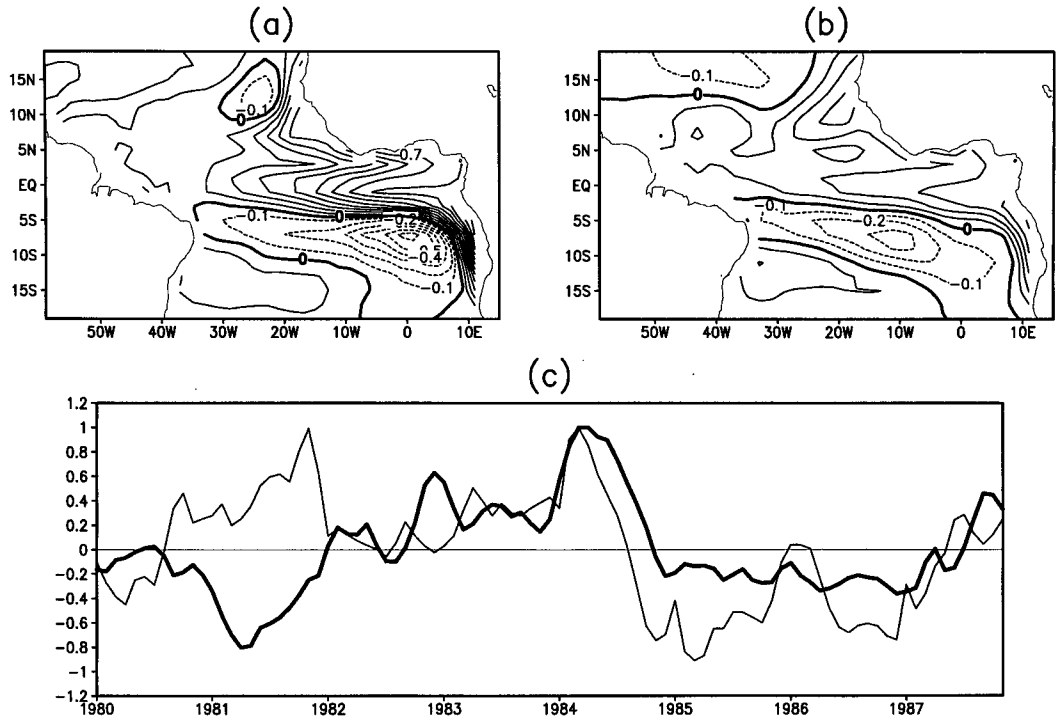

FIG. 19. The second EOF modes of the HC anomalies during 1980–87 in the tropical Atlantic Ocean for (a) the E-winds and (b) the S-winds simulation. The principal components of these modes are presented in (c). The thick line in (c) is for the E-winds simulation and the thin line is for the S-winds simulation. The contour interval for (a) and (b) is 0.1°C.

of the S-winds, especially in winter hemisphere. The strongest southeast trade winds are also shifted to the east in the E-winds in comparison with the S-winds. Around the ITCZ, the E-winds are more zonally oriented so that the convergence zone is not as clearly defined.

Statistical analyses of the wind stress anomalies from both datasets shows that the interannual variability over the tropical Atlantic Ocean in 1980–87 is dominated by a nearly out of phase low-frequency change of the two trade wind systems. Specifically, the southeast trade winds were anomalously strong during 1981–83, but weak during 1984–1986. The northeast trades, on the other hand, were gradually strengthening from 1980–86 with positive anomalies prevailing during 1980–83 and negative anomalies in 1984–86. Superimposed on the low-frequency changes are fluctuations with timescales of months, which also show close agreement between the datasets in the tropical north Atlantic Ocean.

Although there is general agreement, there are also interesting differences in the details of the SVD modes between the two analyses. For instance, there is a clear trend of decreasing wind in the Southern Ocean in the E-winds during 1981–84, where the weakening of the easterly winds was gradual. This is not the case in the S-winds, where the pattern of anomalies is switched abruptly in 1984. Another difference is in the spatial structure of the interannual modes, which shows the lack of fluctuations over the central and eastern part of the tropical south and the equatorial Atlantic in the S-winds. Considering the fact that the observations in these regions are sparse, we suspect that these structural differences reflect different interpolation schemes. Moreover, the interannual signals as revealed by these statistical analyses are much weaker in the S-winds than in the E-winds and the S-winds show much more fluctuations in smaller spatial and temporal scales. It turns out that these differences are not negligible in considering the response of ocean to the wind forcings in interannual scales.

Both datasets of the surface wind stress were used to force an ocean general circulation model. By examining the simulated SST and HC fields, the model sensitivity to wind uncertainty as exemplified by the two datasets is studied. The results have quite different implications for the mean annual state and interannual variability.

For the mean state and its annual cycle, the OGCM experiments show quantitative differences in the simulated ocean thermal state. In comparison with the S-winds simulation, the E-winds simulation produces a shallower thermocline in the Gulf of Guinea, but deeper

thermocline in the western equatorial ocean to the north of the equator and the central and western part of the tropical south Atlantic Ocean. The magnitudes of the differences in the Gulf of Guinea and the western equatorial ocean become larger from boreal fall to winter.

However, the systematic errors of both model simulated SST and HC are not changed significantly with different surface wind forcings. In both simulations, mean SSTs are too cold in the central and eastern equatorial ocean but too warm in the subtropics. The simulated HCs, however, are much colder than the observations in tropical north Atlantic between 10° and 20°N but warmer within 10°S–10°N. Since these errors are not sensitive to the wind disturbances as given by the substantial difference of the two datasets, we may argue that errors in wind forcing are not the major source of the systematic errors of the model mean climatology. Meridional heat transport within the ocean, which strongly depends on the intensity of the western boundary current and hence on model resolution, may be more important.

The model interannual variability, on the other hand, is very sensitive to the uncertainty of wind forcings. This sensitivity is demonstrated by the large differences between the two runs in both the SST and HC anomalies. The EOF analysis of the simulated HC anomalies further shows that oceanic responses generated by the two wind forcings are significantly different. In fact, our comparison between simulations and observations suggests that accurate wind observations are crucial for simulating the SST anomalies because best agreement between the simulations and the observations are in the tropical north Atlantic Ocean where the wind data also have the best agreement and the two simulations are closest to each other. On the other hand, there is little resemblance between the two runs in areas where the model errors in simulating SST anomalies are large.

A projection of the simulated SST anomalies onto the leading EOF modes of the observed anomalies shows that large-scale low-frequency fluctuation of the observed SST anomalies can be reproduced reasonably well by the OGCM simulations. Moreover, we find that the gradual change of the wind stress in the south during 1981–84, as depicted by the E-winds, is superior to the S-winds because the OGCM forced with the E-winds produces a better simulation of the SST anomalies. The strengthening of the northeast trades during 1980–86, as shown from both datasets, is also consistent with a similar trend in the observed and the model simulated SST anomalies. However, as judged by the comparison between the observed and simulated SST anomalies, the E-winds are clearly poor in the early years. In particular, a sudden strengthening of the southeast trades in the E-winds produces an intense cold event in the OGCM during 1981. Instead, both the observations and the S-winds simulation show positive SST anomalies in the equatorial eastern ocean during that year.

Acknowledgments. The authors would like to thank Dr. J. Servain for providing the pseudo-wind stress analyses over the tropical Atlantic Ocean and Professor J. A. Carton for valuable suggestions during the progress of this work and comments on an earlier version of this paper. We would also like to thank Dr. B. Kirtman for comments on the manuscript. We acknowledge Dr. W. G. Large for providing a program on calculating surface drag coefficient, Drs. P. Nobre and S. Schubert for making wind data available, and Ms. T. Yeargin for editing the manuscript. This work was supported by NSF Grant ATM-9019296 and NOAA Grant NA26-GP0149.

REFERENCES

Anderson, D., A. Hollingsworth, S. Uppala, and P. Woiceshyn, 1991: A study of the use of scatterometer data in the European Centre for Medium-Range Weather Forecasts Operational Analysis-Forecast model I. Quality control and validation. *J. Geophys. Res.*, **96,** 2619–2634.

Bengtsson, L., and J. Shukla, 1988: Integration of space and in situ observations to study global climate change. *Bull. Amer. Meteor. Soc.*, **69,** 1130–1143.

Böttger, H., 1982: Local weather element guidance from the ECMWF forecasting system in the medium range. *A Verification Study. Seminar/Workshop 1982 Interpretation of Numerical Weather Prediction Products,* ECMWF, 417–441.

Bretherton, C. S., C. Smith, and J. M. Wallace, 1992: An intercomparison of methods for finding coupled patterns in climate data. *J. Climate,* **5,** 541–560.

Bunker, A. F., 1976: Computation of surface energy flux and annual air–sea interaction cycles of the North Atlantic Ocean. *Mon. Wea. Rev.*, **104,** 1122–1140.

Carton, J. A., and B. Huang, 1994: Warm events in the tropical Atlantic. *J. Phys. Oceanogr.*, **24,** 888–903.

Cayan, D. R., 1992: Variability of latent and sensible heat fluxes estimated using bulk formulae. *Atmos.–Ocean,* **30,** 1–42.

Gent, P., 1991: The heat budget of the TOGA COARE domain in an ocean model. *J. Geophys. Res.*, **96,** 3323–3330.

Goldenberg, S. B., and J. J. O'Brien, 1981: Time and space variability of tropical Pacific wind stress. *Mon. Wea. Rev.*, **109,** 1190–1207.

Halpern, D., 1988: On the accuracy of monthly mean wind speeds over the equatorial Pacific. *J. Atmos. Oceanic Technol.*, **5,** 362–367.

Harrison, D. E., 1989: On climatological monthly mean wind stress and wind stress curl fields over the World Ocean. *J. Climate,* **2,** 57–70.

——, W. S. Kessler, and B. S. Giese, 1989: Ocean circulation model hindcasts of the 1982–83 El Niño: Thermal variability along the ship of opportunity tracks. *J. Phys. Oceanogr.*, **19,** 397–418.

Hellerman, S., and M. Rosenstein, 1983: Normal monthly wind stress over the World Ocean with error estimates. *J. Phys. Oceanogr.*, **13,** 1093–1104.

Hollingsworth, A., D. B. Shaw, P. Lönnberg, L. Illam, K. Arpe, and A. J. Simmons, 1986: Monitoring of observations and analysis quality by a data-assimilation system. *Mon. Wea. Rev.*, **114,** 861–879.

Huang, B., 1992: Numerical simulation of the seasonal and interannual variability of the tropical Atlantic ocean circulation. Ph.D. dissertation, University of Maryland, 210 pp.

——, J. A. Carton, and J. Shukla, 1995: A numerical simulation of the variability in the tropical Atlantic Ocean, 1980–88. *J. Phys. Oceanogr.*, **24,** 835–854.

Janssen, P. A. E. M., P. Lionello, M. Reistad, and A. Hollingsworth, 1989: Hindcasts and data assimilation studies with the WAM model during the Seasat period. *J. Geophys. Res.*, **94,** 973–993.

Kalnay, E., and R. Jenne, 1991: Summary of the NMC/NCAR reanalysis workshop of April 1991. *Bull. Amer. Meteor. Soc.,* **72,** 1897–1904.

Kutzbach, J. E., 1967: Empirical eigenvectors of sea level pressure, surface temperature, and precipitating complexes over North America. *J. Appl. Meteor.,* **6,** 791–802.

Lamb, P. J., 1978a: Large-scale tropical Atlantic surface circulation patterns associated with subsuharan weather anomalies. *Tellus,* **30,** 240–251.

——, 1978b: Case studies of tropical Atlantic surface circulation pattern during recent sub-Sahara weather anomalies, 1967–1968. *Mon. Wea. Rev.,* **106,** 282–291.

——, R. A. Peppler, and S. Hastenrath, 1986: Interannual variability in the tropical Atlantic. *Nature,* **322,** 238–240.

Lanzante, J. R., 1984: A rotated eigenanalysis of the correlation between 700-mb heights and sea surface temperatures in the Pacific and Atlantic. *Mon. Wea. Rev.,* **112,** 2270–2280.

Large, W. G., and S. Pond, 1981: Open ocean momentum flux measurements in moderate to strong winds. *J. Phys. Oceanogr.,* **11,** 324–336.

——, and ——, 1982: Sensible and latent heat flux measurements over the oceans. *J. Phys. Oceanogr.,* **12,** 464–482.

Levitus, S., 1982: *Climatological Atlas of the World Ocean.* NOAA Prof. Paper No. 13, U.S. Govt. Printing Office, Washington, D.C., 183 pp.

Merle, J., 1980: Seasonal heat budget in the equatorial Atlantic Ocean. *J. Phys. Oceanogr.,* **10,** 464–469.

Mestas-Nuñez, A. M., D. B. Chelton, M. H. Freilich, and J. G. Richman, 1994: An evaluation of ECMWF-based climatological wind stress fields. *J. Phys. Oceanogr.,* **24,** 1532–1549.

Miller, A. J., T. P. Barnett, and N. E. Graham, 1993: A comparison of some tropical ocean models: Hindcast skill and El Niño evolution. *J. Phys. Oceanogr.,* **23,** 1567–1591.

Moore, D. W., P. Hisard, J. P. McCreary, J. Merle, J. J. O'Brien, J. Picaut, J.-M. Verstrate, and C. Wunsch, 1978: Equatorial adjustment in the eastern Atlantic. *Geophys. Res. Lett.,* **5,** 637–640.

Moura, A. D., and J. Shukla, 1981: On the dynamics of the droughts in northeast Brazil: Observations, theory, and numerical experiments with a general circulation model. *J. Atmos. Sci.,* **38,** 2653–2675.

Pacanowski, R. C., and S. G. H. Philander, 1981: Parameterization of vertical mixing in numerical models of tropical oceans. *J. Phys. Oceanogr.,* **11,** 1443–1451.

Paolino, D. A., Q. Yang, B. Doty, J. L. Kinter III, J. Shukla, and D. M. Straus, 1995: A pilot reanalysis project at COLA. *Bull. Amer. Meteor. Soc.,* **76,** 697–710.

Philander, S. G. H., and R. C. Pacanowski, 1986: A model of the seasonal cycle in the tropical Atlantic Ocean. *J. Geophys. Res.,* **91,** (C12), 14 192–14 206.

——, W. J. Hurlin, and A. D. Siegel, 1987: Simulation of the seasonal cycle of the tropical Pacific Ocean. *J. Phys. Oceanogr.,* **17,** 1986–2002.

Picaut, J., J. Servain, P. Lecomte, M. Seva, S. Lukas, and G. Rougier, 1985: Climate atlas of the tropical Atlantic wind stress and sea surface temperature 1964–1979. Université de Bretagne Occidentale—University of Hawaii, 467 pp.

Prohaska, J., 1976: A technique for analyzing the linear relationships between two meteorological fields. *Mon. Wea. Rev.,* **104,** 1345–1353.

Rebert, J. P., J. R. Donguy, G. Eldin, and E. Wyrtki, 1985: Relations between sea level, thermocline depth, heat content, and dynamic height in the tropical Pacific Ocean. *J. Geophys. Res.,* **90,** 11 719–11 725.

Reverdin, G., P. Delécluse, C. Lévy, P. Andrich, A. Morlière, and J. M. Verstraete, 1991: The near surface tropical Atlantic in 1982–1984: Results from a numerical simulation and a data analysis. *Progress in Oceanography,* Vol. 22, Pergamon, 273–340.

Reynolds, R. W., K. Arpe, C. Gordon, S. P. Hayes, A. Leetmaa, and M. J. McPhaden, 1989: A comparison of tropical Pacific surface wind analyses. *J. Climate,* **2,** 105–111.

Rosati, A., and K. Miyakoda, 1988: A general circulation model for upper ocean simulation. *J. Phys. Oceanogr.,* **18,** 1601–1626.

Schubert, S. D., R. B. Rood, and J. Pfaendtner, 1993: An assimilated dataset for earth science applications. *Bull. Amer. Meteor. Soc.,* **74,** 2331–2342.

Seager, R., S. E. Zebiak, and M. A. Cane, 1988: A model of the tropical Pacific sea surface temperature climatology. *J. Geophys. Res.,* **93,** 1265–1280.

Servain, J. J., 1991: Simple climatic indices for the tropical Atlantic Ocean and some applications. *J. Geophys. Res.,* **96,** 15 137–15 146.

——, and D. M. Legler, 1986: Empirical orthogonal function analysis of tropical Atlantic sea surface temperature and wind stress: 1964–1979. *J. Geophys. Res.,* **91,** 14 181–14 191.

——, J. Picaut, and J. Merle, 1982: Evidence of remote forcing in the equatorial Atlantic Ocean. *J. Phys. Oceanogr.,* **12,** 457–463.

——, ——, and A. J. Busalacchi, 1985: Interannual and seasonal variability of the tropical Atlantic Ocean depicted by sixteen years of sea surface temperature and wind stress. *Coupled Ocean Models,* J. C. J. Nihoul, Ed., Elsevier, 211–237.

——, M. Seva, S. Lukas, and G. Rougier, 1987: Climatic atlas of the tropical Atlantic wind stress and sea surface temperature: 1980–1984. *Ocean–Air Interact.,* **1,** 109–182.

Trenberth, K. E., 1992: Global analyses from ECMWF and atlas of 1000 to 10 mb circulation statistics. NCAR Tech. Note NCAR/TN 373, 191 pp.

——, and J. G. Olson, 1988: An evaluation and intercomparison of global analyses from the National Meteorological Center and the European Centre for Medium-Range Weather Forecasts. *Bull. Amer. Meteor. Soc.,* **69,** 1047–1057.

——, W. G. Large, and J. G. Olson, 1989a: The effective drag coefficient for evaluating wind stress over the oceans. *J. Climate,* **2,** 1507–1516.

——, ——, and ——, 1989b: A global ocean wind stress climatology based on ECMWF analyses. NCAR Tech. Note NCAR/TN338, 93 pp.

——, ——, and ——, 1990: The mean annual cycle in global ocean wind stress. *J. Phys. Oceanogr.,* **20,** 1742–1760.

Wallace, J. M., C. Smith, and C. S. Bretheton, 1992: Singular value decomposition of winter sea surface temperature and 500-mb height anomalies. *J. Climate,* **5,** 561–576.

Wyrtki, K., and G. Meyers, 1976: The trade wind field over the Pacific Ocean. *J. Appl. Meteor.,* **15,** 698–704.